NACA

RESEARCH MEMORANDUM

EXPERIMENTAL DAMPING IN PITCH OF 45° TRIANGULAR WINGS

By Murray Tobak, David E. Reese, Jr.,
and Benjamin H. Beam

Ames Aeronautical Laboratory
Moffett Field, Calif.

NATIONAL ADVISORY COMMITTEE FOR AERONAUTICS

WASHINGTON
December 1, 1950

NATIONAL ADVISORY COMMITTEE FOR AERONAUTICS

RESEARCH MEMORANDUM

EXPERIMENTAL DAMPING IN PITCH OF 45° TRIANGULAR WINGS

By Murray Tobak, David E. Reese, Jr.,
and Benjamin H. Beam

SUMMARY

The results of an experimental wind-tunnel investigation of the damping in pitch of two triangular wings having leading edges swept back 45° are presented. The wings differed only in airfoil section, one wing having a sharp leading-edge biconvex section, the other a round leading-edge section, NACA 0006-63. The investigation, which was conducted over a Mach number range of 1.15 to 1.70, consisted of tests made of the isolated wings and of the wings in combination with a slender body. The results of a similar investigation for one of the wing-body combinations, made over a Mach number range of 0.23 to 0.94, are also reported herein.

The results, obtained by a single-degree-of-freedom oscillation technique, were in qualitative agreement with the results of theoretical computations for both subsonic and supersonic speeds. The prediction by the supersonic theory of the existence of ranges of Mach number and center-of-gravity positions over which dynamic instability may be expected was confirmed by the experimental results.

A significant reduction of the range of Mach numbers over which negatively damped oscillations were encountered was obtained by removing the tips of the wings.

Application of the theory to a study of the coupled two-degrees-of-freedom short-period pitching motion of a tailless triangular-wing aircraft at supersonic speeds is discussed.

INTRODUCTION

In an effort to surmount the problems which arise with flight at transonic or supersonic speeds, many unconventional wing plan forms have been proposed. One of these, the delta or triangular wing, has shown

considerable promise and therefore has been the subject of extensive theoretical and experimental investigations. One of these theoretical investigations (reference 1) has shown that, over certain Mach number ranges and for certain center-of-gravity positions, dynamic instability in the form of negatively damped oscillations of the short-period pitching motion is to be expected. A later paper (reference 2) presented a similar theoretical result.

Since the theory is based on linearized equations for the flow of an inviscid fluid, it is possible that second-order thickness and viscous effects may significantly alter the results. Further, the theoretical treatments are for quasi-stationary flow (reference 2), that is, for relatively slow oscillations.

In view of these limitations of the theory, an investigation has been undertaken in the Ames 6- by 6-foot supersonic wind tunnel for the purpose of determining the accuracy of the theory in predicting the dynamic behavior of wings and wing-body combinations in flight. The present report is devoted to an experimental investigation of the damping of single-degree-of-freedom pitching oscillations of triangular wings and wing-body combinations about a lateral axis lying within the wings. The report includes the results of a similar limited investigation made at subsonic speeds in the Ames 12-foot pressure tunnel employing one of the models used in the investigation at supersonic speeds.

NOTATION

A aspect ratio $\left(\frac{b^2}{S}\right)$

B cotangent of Mach angle $\left(\sqrt{M^2-1}\right)$

C_L lift coefficient $\left(\frac{\text{lift}}{\frac{1}{2}\rho V^2 S}\right)$

C_m pitching-moment coefficient $\left(\frac{\text{pitching-moment}}{\frac{1}{2}\rho V^2 S\bar{c}}\right)$

I moment of inertia, slug-feet squared

K restoring moment per unit angular deflection, foot-pounds per radian

M Mach number $\left(\frac{V}{\text{speed of sound}}\right)$

P	damping moment per time rate of change of angle of attack, foot-pound-seconds
R	Reynolds number, based on wing mean aerodynamic chord
S	wing area, including portion enclosed by body, square feet
V	flight speed, feet per second
b	wing span, feet
c	wing root chord, feet
$\bar{c}$	wing mean aerodynamic chord $\left[\bar{c} = \frac{2}{S} \int_0^{b/2} (\text{local chord})^2 \, dy \right]$, feet
e	base of natural logarithms
f	frequency of oscillation, cycles per second
q	angular velocity due to pitching, radians per second
t	time, seconds
$x_{a.c.}$	chordwise distance of the aerodynamic center behind the leading edge of the mean aerodynamic chord
$x_{c.g.}$	chordwise distance of the center of gravity behind the leading edge of the mean aerodynamic chord.
$\Delta x_{c.g.}$	$x_{a.c.} - x_{c.g.}$
y	spanwise coordinate, measured from line of symmetry of wing, feet
α	angle of attack of wing center line, degrees
ϵ	semivertex angle of wing plan form, degrees
μ	Mach angle ($\sin^{-1} 1/M$), degrees
ρ	mass density of air, slugs per cubic foot
ω	angular frequency of oscillation ($2\pi f$), radians per second

When α, q, and $\dot{\alpha}$ are used as subscripts, a nondimensional derivative is indicated and this derivative is evaluated as the independent variable (α, $\dot{\alpha}$, q) approaches zero. For example:

$$C_{m_\alpha} = \left(\frac{\partial C_m}{\partial \alpha}\right)_{\alpha \longrightarrow 0} \qquad C_{m_q} = \left[\frac{\partial C_m}{\partial (q\bar{c}/2V)}\right]_{q \longrightarrow 0}$$

$$C_{m_{\dot{\alpha}}} = \left[\frac{\partial C_m}{\partial (\dot{\alpha}\bar{c}/2V)}\right]_{\dot{\alpha} \longrightarrow 0}$$

A dot above a symbol denotes a derivative with respect to time. Angles, forces, and moments are referred to the center of gravity of the wing and are positive as indicated in figure 1.

In addition to the preceding notation, which is used in the body of the report, the following notation is used in the appendices:

Appendix A

$\bar{C}_{L_1}(D)$	operational form of indicial lift coefficient
$C_{L_{q_{a.c.}}}$	rate of change of lift coefficient with the parameter $q\bar{c}/2V$ for pitching about the wing aerodynamic center
C_{m_b}	pitching-moment coefficient due to effective twist
C_{m_c}	pitching-moment coefficient due to effective camber
$C_{m_{q_o}}$	pitching-moment coefficient due to pitching when the lift due to pitching is zero
F(n),G(n)	indicial lift constants evaluated for elliptic wings
c_l	local chord, spanwise distance y from root chord
i	$\sqrt{-1}$
n	$\frac{\omega\bar{c}}{2V}$

s	distance traveled in half mean aerodynamic chord lengths $\left(s = \frac{Vt}{\bar{c}/2}\right)$
$(\alpha_r)_o$	angle of attack of the three-quarter-chord point of the root section mean line when the lift due to pitching is zero
β	camber function $2 \times \left(\frac{\text{maximum height of camber line}}{\text{chord}}\right)$
ϵ	total spanwise twist, measured at the three-quarter-chord line, positive when root section is at greater angle of attack than tip section

Appendix B

B_b	body base cross-sectional area
B_m	body mean cross-sectional area
a	local body radius
$\bar{a}$	local speed of sound
l	body length
w	vertical velocity of body
$\bar{x}$	distance of centroid of body volume from nose $\left(\bar{x} = \frac{\int_o^l \pi a^2 x dx}{B_m l}\right)$
x_o	distance of axis of rotation of body from nose
x,y,z	rectangular coordinates (sketch, page 29)
Δp	local loading on surface of body
φ	velocity potential

Appendix C

D	$\frac{d}{dt}$
$T_{1/2}$	time for an oscillation to decrease to one-half amplitude

k	$\frac{2I}{\rho V^2 S\bar{c}}$
m	aircraft mass
γ	inclination of aircraft flight path with respect to horizontal axis (sketch, page 35)
θ	attitude of aircraft with respect to horizontal axis (sketch, page 35)
τ	$\frac{m}{\rho V S}$
ψ	damping parameter

APPARATUS

Wind Tunnel

The experimental investigation of the damping-in-pitch characteristics of the triangular wing models at supersonic speeds was conducted in the Ames 6- by 6-foot supersonic wind tunnel. This tunnel is of the closed-return variable-pressure type with a Mach number range of 1.15 to 2.0. A complete description of the wind tunnel is given in reference 3.

Subsonic tests of one of these models were performed in the Ames 12-foot pressure wind tunnel. This tunnel, also of the closed-return variable-pressure type, is capable of attaining air-stream velocities close to the speed of sound.

Model

Two triangular wings with leading edges swept back 45° were used in the investigation. Their pertinent dimensions are shown in figure 2. The wings were identical except for airfoil section, one wing having a sharp leading-edge biconvex section (see reference 4), the other a round leading-edge section, NACA 0006-63. Both sections were symmetrical in streamwise planes and 6 percent thick at their 30-percent chord lines. The maximum size of the model was limited by tunnel-wall interference effects, this limitation dictating a wing span of 30 inches. Both models were constructed of wood over a thin steel spar. The reduction in moment of inertia obtained by the wood construction permitted the use of a spring

support system of reasonable stiffness. The wing tips were reinforced with strips of brass to minimize the possibility of elastic deformation of the tips under load.

During the first series of tests, the model was fitted with a conical shroud of 30° included angle in order to shield the spring support system. The dimensions of the shroud and its location on the wing are shown in figure 2.

For the second series of tests, a slender body of the shape derived by Haack in reference 5 was fitted to the model as shown in figure 3. The body of thin laminated wood construction extended 15 inches ahead of the wing apex and terminated at the wing trailing edge. Its maximum diameter was 4 inches, giving a ratio of wing span to body diameter of 7.5. A photograph of the triangular-wing-body combination installed in the Ames 6- by 6-foot supersonic wind tunnel is shown in figure 4.

For the third series of tests, the tips of the wings were cut off, reducing the model span from 30 inches to 24 inches, the wing aspect ratio from 4 to 2.67, and the ratio of wing span to body diameter from 7.5 to 6.

Model Support System

In this investigation, the damping in pitch was obtained by measuring the decay of a free oscillation of the model. The model was therefore mounted on spring supports proportioned to give a frequency of about 10 cycles per second. The equivalent reduced frequency is essentially the frequency of the short-period oscillations usually experienced in dynamic stability studies of full-scale aircraft and missiles.

As shown in figure 5, the model was mounted in a flexure pivot system consisting of two thin vertical pivots which restrained the model in vertical motion but offered little resistance to rotation and a long, flat, horizontal spring which restrained the model in rotation and horizontal motion. The latter spring was equipped with a strain gage so that a recording oscillograph could be used to produce a record of displacement of the model as a function of time. Flexure pivots were used for the spring support system since with this method the only damping due to friction was that caused by the internal friction of the pivots themselves. This quantity remained essentially constant throughout the period of test.

The model was given an initial displacement of 7° by means of a pawl which engaged the wing in the course of its arc, deflected the wing and swung past, permitting the model to oscillate freely. The pawl was operated through the linkage system shown in figure 5 by a pneumatically

actuated piston in the sting support. A positive lock to restrain any violent oscillations was also provided. This lock, not illustrated in figure 5 for reasons of clarity, was also operated by a pneumatic piston.

THEORY

For the single degree-of-freedom oscillations of this investigation the damping coefficients presented are, in the terminology of reference 1, the sum of the damping due to pitching velocity C_{m_q} and the damping due to the rate of change of angle of attack with time $C_{m_{\dot{\alpha}}}$. In this single test, these derivatives cannot be separated.

Triangular Wing

Supersonic theory.- The theory of reference 1 is applicable in the range of supersonic Mach numbers for which the Mach lines are swept ahead of the wing leading edge. For higher Mach numbers, where the Mach lines are swept behind the wing leading edge, the theory developed by Miles in reference 2 was used. For this case, in the notation of the present report, the damping in pitch about an arbitrary pitching axis is

$$C_{m_q} + C_{m_{\dot{\alpha}}} = -\frac{1}{2B}\left(2 - \frac{1}{B^2}\right) + \frac{\Delta x_{c.g.}}{\bar{c}}\left(\frac{4}{B^3}\right) - \frac{8}{B}\left(\frac{\Delta x_{c.g.}}{\bar{c}}\right)^2$$

It is interesting to note that Miles' results for the case wherein the Mach lines are swept ahead of the leading edge, developed by a different procedure, concur with the theoretical results of reference 1 for the sum of C_{m_q} and $C_{m_{\dot{\alpha}}}$.

Subsonic theory.- The stability derivative C_{m_q} is defined as the pitching-moment coefficient due to steady pitching so that it is possible to calculate its magnitude by using the subterfuge of replacing the thin flat wing in pitching flight with a thin cambered and twisted wing in straight flight. The charts and tables of references 6 and 7 may then be used to determine the lift and pitching-moment characteristics of such a cambered and twisted wing.

Approximate values of $C_{m_{\dot{\alpha}}}$ were calculated from expressions for unsteady or indicial lift, developed in reference 8. The Prandtl-Glauert

rule for the effect of compressibility was applied to the values of C_{m_q} and $C_{m_{\dot{\alpha}}}$ calculated by the preceding methods. A detailed presentation of the method of obtaining C_{m_q} and $C_{m_{\dot{\alpha}}}$ at subsonic speeds is given in appendix A.

Triangular Wing With Cut-Off Tips

Since the experimental damping in pitch of the triangular wing with cut-off tips was not investigated at subsonic speeds, only the theoretical results for this wing at supersonic speeds with Mach lines swept ahead of the leading edges are presented. The theoretical values for C_{m_q} and $C_{m_{\dot{\alpha}}}$ at supersonic speeds for this wing were calculated by integrating the appropriate local loadings over regions I and II of the wing shown in figure 6. The pressure-coefficient terms were obtained from table 1 of reference 9. The damping-in-pitch contribution of region III in figure 6 was neglected, since it is known that regions influenced by the wing-tip Mach cone contribute very little to the total load.

Body

The contribution of the body to the damping in pitch was calculated using Munk's slender body theory (reference 10) in a manner similar to that used by Ribner in reference 11 to obtain the stability derivatives of low aspect-ratio triangular wings. The development is given in appendix B. The result of the analysis concurs with that given by Miles in reference 12.

Because of the large ratio of wing span to body diameter, the interference effects between the wing and body were thought to be negligible, so that only the damping contribution of the portion of the body ahead of the wing apex was considered. Also, since the theoretical expression for the damping of the body is essentially independent of Mach number, the results developed in appendix B were used for both subsonic and supersonic speeds.

EXPERIMENT

Scope of Tests

Supersonic tests in the Ames 6- by 6-foot supersonic wind tunnel.- Investigation of the damping-in-pitch characteristics of triangular wings

at supersonic speeds was conducted over a Mach number range of 1.15 to 1.70 at a constant tunnel absolute pressure of 5 pounds per square inch. The Reynolds number ranged from 1.23 million to 1.35 million, based on the wing mean aerodynamic chord.

The models were oscillated about nominal angles of attack of 0° and 5°, the angles being measured from the mean line of the sting support to the axis of the test section.

The various model configurations, each of which was investigated employing the airfoil sections shown in figure 2, are indicated below:

Model configuration	Range of moment of inertia (slug $-ft^2$)	Axis of rotation (% M.A.C.)	Range of wind-on frequency (cps)
Wing alone	0.0124 –0.0127	45	10–13
Wing and shroud	.0216 –.0232	45	11–13
Wing and body	.0376 –.0389	45	6–10
Wing and body	.0311 –.0319	35	11–14
Wing with cut-off tips and body	.0310 –.0315	47.5 (equivalent to triangular wing axis at 0.35 $\bar{c}$)	10–13

Subsonic tests in the Ames 12-foot pressure wind tunnel.– Subsonic tests of the round leading-edge section NACA 0006-63 triangular wing with body attached were performed over a Mach number range of 0.23 to 0.94 at constant Reynolds numbers of 1.23 million and 0.55 million. For these tests, the model was pivoted at an axis of rotation located at 35 percent M.A.C. and was oscillated about a mean angle of attack of 0°.

Reduction of Data

The technique used in this experiment of pivoting the model about a lateral axis and allowing it to perform pitching oscillations about that axis enabled the aerodynamic damping coefficient to be determined from the record of the oscillation-decay curve, after correction had been made for the damping provided by the internal friction of the supporting springs.

The motion described previously may be expressed as a linear differential equation

$$I\ddot{\alpha} + P_2\dot{\alpha} + K_2\alpha = 0 \qquad (1)$$

Each of these quantities defines a moment: the first due to the angular acceleration of the model mass, the second due to aerodynamic and friction damping forces, and the third due to mechanical and aerodynamic restoring forces.

The total damping P_2 is written as $P_2 = P_o + P_1$

where

P_o aerodynamic damping

P_1 tare damping due to the internal friction of the supporting springs

Then the aerodynamic damping moment is $-(P_2-P_1)\dot{\alpha}$ which when reduced to coefficient form becomes

$$C_m = \frac{-(P_2-P_1)\dot{\alpha}}{\frac{1}{2}\rho V^2 S\bar{c}} \qquad (2)$$

Writing the moment coefficient in the form of the parameter used in dynamic stability work $\left[\frac{\partial C_m}{\partial(\dot{\alpha}c/2V)}\right]$ gives

$$C_{m_q} + \dot{C}_{m_{\dot{\alpha}}} = \frac{-4(P_2-P_1)}{\rho V S\bar{c}^2} \qquad (3)$$

Thus, it is seen that it is only necessary to evaluate P_2 and P_1 in order to obtain the damping derivative.

If in equation (1) the conditions $\alpha=\alpha_o$ and $\dot{\alpha}=0$ exist at time $t=0$, the equation describing the model angle of attack as a function of time may be written as

$$\alpha=\alpha_o e^{-(P_2/2I)t}\left(\cos \omega t + \frac{P_2}{2I\omega} \sin \omega t\right) \qquad (4)$$

where ω is the angular frequency of oscillation, and is given by

$$\omega = \sqrt{(K_2/I)-(P_2/2I)^2} \tag{5}$$

The envelope curve for equation (4) is

$$\alpha = \alpha_o e^{-(P_2/2I)t} \tag{6}$$

where P_2 is a constant which may be determined as

$$P_2 = \frac{2I}{\Delta t} \ln\left(\frac{\alpha_o}{\alpha}\right) \tag{7}$$

where α_o and α are ordinates of the envelope curve, a time interval Δt apart. It was found, however, that due to some nonlinearity inherent in the spring support system P_2 was not a constant but was dependent to a small degree on the amplitude of oscillation. It was evident from the results of wind-off tests, made with the wind tunnel evacuated to a low pressure, that the nonlinearity was of mechanical, not of aerodynamic nature. To minimize its effect, the same initial amplitude and the same amplitude range was used in the reduction of all records. It was then always possible to draw a reasonable straight line through the experimental points when the amplitudes of the envelope curve were plotted on semi-logarithmic paper as a function of time. A typical oscillation record and plot of the envelope curve is shown in figure 7.

The tare damping P_1 was obtained in a like manner by oscillating the model with the wind off through a wind-tunnel pressure range of 15 to 3 pounds per square inch absolute. The resulting curve of tare damping versus tunnel pressure was extrapolated to zero tunnel pressure to obtain the tare damping due to mechanical friction alone, the extrapolation eliminating the effect of air damping. It was usually found, however, that the difference in tare damping at zero and 3 pounds per square inch absolute was negligible.

The wind-off records were also used to determine the frequency in the equation,

$$I = \frac{K_1-P_1^2/4I}{4\pi^2 f^2} \simeq \frac{K_1}{4\pi^2 f^2} \tag{8}$$

so that the moment of inertia of the model could then be determined. The quantity K_1 is the spring constant of the support system obtained by a static calibration.

The variation of pitching-moment coefficient with angle of attack C_{m_α} was also obtained from the oscillation records since the frequency is a function of the sum of the spring constant and the aerodynamic restoring moment. The total restoring moment per unit angle of attack is written as

$$K_2 = K_0 + K_1$$

where

K_0 aerodynamic restoring moment for unit angle of attack

K_1 calibrated static spring constant

Then the aerodynamic restoring moment is $-(K_2-K_1)\alpha$, which when reduced to coefficient form is

$$C_{m_\alpha} = \frac{dC_m}{d\alpha} = \frac{-2(K_2-K_1)}{\rho V^2 S\bar{c}} \tag{9}$$

The quantity K_2 was obtained by measuring the frequency of oscillation of the model from the wind-on records and use of equation (5).

Precision of Data

As noted previously, reduction of an oscillation-decay curve to coefficient form involves the measurement of the exponents of the wind-on and wind-off envelope curves, the model moment of inertia, and the density and velocity of the air stream. The accuracy with which these quantities can be determined may be considered to be a function of those factors involved in their determination. In the following analysis of the precision, the results apply to the data obtained at subsonic speeds as well as at supersonic speeds.

The uncertainty in determining the exponent of a decay curve was taken to be the standard deviation resulting from repeated measurements for the exponent of a single record. The same uncertainty, found to be ±0.008 per second, existed for both wind-on and wind-off records.

Uncertainties in the density and velocity of the air stream were determined from the least readings of the instruments measuring the tunnel stagnation temperature and pressure. These were ±2° F for the stagnation temperature gage and ±0.2 centimeter for the mercury manometer measuring stagnation pressure, which led to uncertainties of ±0.01 percent and ±0.9 percent for the density and velocity, respectively.

The uncertainty in the value for the moment of inertia of the model was primarily dependent upon the accuracy with which the wind-off frequency of oscillation could be determined. Repeated measurements of the frequency of oscillation of a single wind-off record gave a standard deviation of ±0.015 cycle per second. This uncertainty, together with an uncertainty of ±14 inch-pounds per radian in the spring constant, gave a total uncertainty in the moment of inertia of the model of ±1.5 percent.

The total uncertainty in the damping coefficient ($C_{m_{\dot{\alpha}}} + C_{m_q}$) was then taken to be the square root of the sum of the squares of the aforementioned uncertainties, this computation resulting in a value of ±0.02.

There remains the necessity of discussing those factors which, either systematically or erratically, might have influenced the damping of the model in such a manner as to mask the trends of the damping coefficients or to induce self-excited oscillations.

Random errors, exhibited by the scatter in the data, were due primarily to indeterminate changes in the friction damping of the spring support system. When it is considered that friction forces account for 25 percent of the damping moment, it is evident that only very small changes in the character of the spring support system can produce the scatter apparent in the data. Consequently, although the uncertainty in a single damping coefficient is of the order of ±0.02, the standard deviation of a number of observations at a given Mach number is of the order of ±0.06.

A possible source of systematic error, which subsequently was determined to be negligible, was that due to the vibration of the model support sting. It was observed that, when the model was given its initial deflection and released, the consequently large and sudden change in lift caused a vibration of the sting support. This vibration, when coupled with the oscillation of the model, could have produced a motion consisting of two degrees of freedom instead of one, with ensuing complication of the equations of motion and methods of analysis. To investigate this possibility, a strain gage was attached to the sting support and connected to a recording oscillograph, enabling a record to be made of the amplitude and frequency of vibration induced in the sting. Upon analysis of the record, it was found that the maximum amplitude of vibration of the sting was ±0.06 inch, causing at most a change of ±0.15° in the angle of attack of the model. In addition to the above analysis, a 22-inch section of the sting was removed, thereby stiffening the sting considerably. The results of tests made with the model mounted on the shortened sting agreed, within the precision mentioned previously, with tests made with the standard sting.

RESULTS AND DISCUSSION

The results of tests of the damping-in-pitch characteristics of the various model configurations are presented in figures 8 to 12. The damping coefficients are given as a function of Mach number, and also at supersonic speeds as a function of the ratio of $\tan \epsilon / \tan \mu$, the ratio of the tangent of the semivertex angle of the wing to the tangent of the Mach angle. Values of $\tan \epsilon / \tan \mu$ greater than one correspond to Mach numbers for which the Mach lines are swept behind the wing leading edge and less than one to Mach numbers for which the Mach lines are swept ahead of the leading edge. The damping coefficients presented are, in the terminology of reference 1, the sum of the damping due to pitching velocity C_{m_q} and the damping due to the rate of change of angle of attack with time $C_{m_{\dot{\alpha}}}$.

Damping Coefficients

Triangular wing at supersonic speeds.- The results of tests of the triangular wing conducted at supersonic speeds are shown in figure 8. For these tests, the model was initially fitted with a conical shroud of 30° included angle in order to shield the spring support system.

Examination of the data for the wing and shroud in figure 8 shows that the experimental points follow the trends predicted by the theoretical results. It is of importance to note that, for the axis of rotation located at 45 percent of the mean aerodynamic chord, the theory indicates positive damping coefficients for a range of Mach numbers less than 1.17. In this speed range, oscillations of increasing amplitude are to be expected for the single degree-of-freedom motion of this investigation. During the tests, these undamped or negatively damped oscillations were observed, as shown in figure 8 by the experimental points plotted below the axis. The reversal from negative to positive damping coefficients occurred at somewhat higher Mach numbers than indicated by the theory.

During these tests, it was suggested that the interference between the shroud and the wing, consisting of an alternate attachment and detachment of the bow wave from the shroud, could have influenced the damping of the model in such a manner as to give the negatively damped oscillations which were observed. In order to investigate this point, further tests were made with the shroud removed. The results, also shown in figure 8, indicate a significant increase in negative damping coefficients in the low Mach number range. However, removal of the shroud exposed a sizable cut-out in the airfoil surface, which, according

to theory, should give an increase in damping. Further, removal of the shroud exposed the spring support to the air stream and may have resulted in serious interference effects. Whether the increase in experimental damping with shroud removed is attributable to the absence of the shroud or to the effect of the cut-out and/or support interference is not known.

In view of the inconclusiveness of the results for the isolated wing due to the possibility of interference between the wing and shroud, a second series of tests was conducted. For these tests, a slender body of efficient aerodynamic shape was fitted to the wing.

The results for the wing-body combination, shown in figures 9 and 10, again follow the trends predicted by the theory, and again ranges of Mach numbers were encountered over which the model experienced negatively damped oscillations. The verification of the existence of these regions of dynamic instability is considered to be the most significant result of this investigation.

A comparison of the data of figures 9 and 10 for the sharp leading-edge section and round leading-edge section (NACA 0006-63) airfoils shows that the sharp leading-edge airfoil more closely followed the theoretical trends and usually gave slightly higher damping. It is felt, however, that the difference in damping was not sufficiently large, nor were the data sufficiently precise to warrant a conclusion regarding the relative merits of the damping qualities of the two airfoils.

Likewise, there appeared to be no consistent significant difference between the magnitudes of the damping coefficients for the model oscillating about 0° and 5° angles of attack.

A comparison of the results for the wing-body combination pivoted at 45 percent M.A.C. (fig. 9) and at 35 percent M.A.C. (fig. 10) showed that, as predicted by the theory, results obtained at 45 percent M.A.C., gave both higher damping at a given Mach number and a smaller range of Mach numbers over which negatively damped oscillations were encountered.

Wing with cut-off tips at supersonic speeds.- Theoretical calculations based on the results of reference 9 have indicated that significant improvement of the damping-in-pitch characteristics of a triangular wing may be realized by employing swept-back trailing edges. Since this improvement is accomplished by reducing the area of the triangular wing aft of the center of gravity, the possibility was suggested that the damping-in-pitch characteristics of the wings of this report could likewise be improved by removing the tips of the wings. The results of calculations for such plan forms (see section on theory) also tended to support this suggestion.

In order to investigate this possibility, the wings of this report were modified as shown in figure 3, removal of the wing tips reducing the aspect ratio of the wings from 4.0 to 2.67. For this investigation, the model was pivoted at 47.5 percent M.A.C., which is the same root-chord position as that for the triangular wing pivoted at 35 percent M.A.C.

Results of the tests made with the modified wings (shown in fig. 11) can thus be compared with those of the triangular wings pivoted at 35 percent M.A.C. (shown in fig. 10). This comparison, which is useful primarily for the purpose of verifying the theory, shows that, as predicted, a significant reduction of the region of Mach numbers over which negatively damped oscillations were encountered was realized as the result of removing the wing tips. It is recognized that a more ideal comparison of the damping-in-pitch characteristics of the two wings would be one in which the axes of the wings were located so as to give equivalent static margins. Structural limitations of the model prevented such an experimental comparison from being made; however, a theoretical comparison on this basis indicated that the wing with cut-off tips possesses superior damping-in-pitch characteristics for all values of static margin, although the improvement is small for static margins less than 0.03.

Triangular wing at subsonic speeds.- In order to obtain a more complete picture of the variation of the damping coefficients with Mach number, the round leading-edge section (NACA 0006-63) triangular wing with body attached was investigated in the Ames 12-foot pressure wind tunnel.

In figure 12, the experimental variation of $C_{m_q} + C_{m_{\dot{\alpha}}}$ with subsonic Mach numbers is presented for a pitching axis located at 35 percent M.A.C., and for Reynolds numbers of 1.25 million and 0.55 million. Examination of figure 12 shows that for both Reynolds numbers the damping coefficients became more negative as the Mach number was increased until a limiting Mach number was reached at which they abruptly became positive. The sudden appearance of this condition of instability is believed to be associated with the establishment of local regions of supersonic flow over the surface of the airfoil.

Also shown in figure 12 are theoretical values of $C_{m_q} + C_{m_{\dot{\alpha}}}$ through the subsonic Mach number range calculated by two different methods. The values calculated using low-aspect-ratio theory (reference 11) indicate no change with Mach number and are numerically much larger than the experimental values. In reference 11, it is pointed out that assumptions made in the derivation limit application of the results to wings of aspect ratio less than 0.5. Thus, the application of values of C_{m_q} and $C_{m_{\dot{\alpha}}}$ obtained from low-aspect-ratio theory to

wings of the aspect ratio of this report for subsonic speeds does not appear to be justified. Values of $C_{m_q} + C_{m_{\dot{\alpha}}}$ obtained using a theory for wings of moderate to high aspect ratio (see section on theory) are shown in figure 12 to agree well with the test results for a Reynolds number of 1.25 million. The abrupt reversal in sign of the damping coefficients is not predicted by the theory, however, since the theory cannot take into account the effect of mixed flow on the damping-in-pitch behavior of the wing.

Aeroelastic Effects at Supersonic Speeds

Since the models of this investigation employed wings having swept-back leading edges, and since the wing tips were relatively flexible, it was thought possible that aeroelastic effects commonly observed on the static lift and pitching-moment coefficients might have similarly influenced the damping coefficients.

In order to investigate this possibility, the static pitching-moment coefficient C_{m_α} was computed by the method outlined in the section of this report entitled "Reduction of Data" for the triangular wing-body combination pivoted at 45 percent M.A.C. Results of these computations for the round leading-edge section NACA 0006-63 wing are shown in figure 13, and for the sharp leading-edge section wing in figure 14. Also shown in figure 13 are unpublished results, obtained in the Ames 6-by 6-foot supersonic wind tunnel, of force tests of a triangular wing-body combination built of steel, having a wing swept back 45° and employing an NACA 0005-63 airfoil section. These results were obtained at the same tunnel pressure as the results of the present report. Since it was known that aeroelastic effects on the comparatively rigid force-test model were negligible, it was expected that the effect of aeroelasticity on the more flexible models of this report would show up as a difference in the parameter C_{m_α} for the two models. Comparison of the results shown in figure 13 at a Mach number of 1.4, where the dynamic pressure and thus any aeroelastic effects are greatest, shows good agreement between the results of the two experiments. It was therefore concluded that, in the present investigation, aeroelastic effects on the static parameter C_{m_α} and also the dynamic parameters C_{m_q} and $C_{m_{\dot{\alpha}}}$ were negligible.

It is interesting to note that the results of the present investigation shown in figures 13 and 14 indicate that the triangular wing-body combination pivoted at 45 percent M.A.C., had become statically unstable at a Mach number of 1.55 for the round leading-edge section NACA 0006-63 wing and 1.46 for the sharp leading-edge section wing.

The fact that this reversal in sign of the pitching-moment coefficient was not observed in the results of the force tests of the wing-body combination may be attributed to the differences in airfoil-section thickness and body shape between the two models. Both of these differences have more pronounced effects on the lift and pitching moment as the Mach number increases.

Reynolds Number Effects

In view of the relatively low Reynolds numbers at which the present tests were conducted, it was deemed advisable to obtain some measure of the effect of Reynolds number on the damping-in-pitch coefficients. Since the maximum Reynolds number was limited to that used in the supersonic investigation (1.35 million) by strength limitations of the model, the investigation of Reynolds number effect could only be made by testing at a lower Reynolds number.

Accordingly, subsonic tests of the damping in pitch of the round leading-edge section NACA 0006-63 triangular wing-body model were made at constant Reynolds numbers of 1.25 million and 0.55 million. The results (fig. 12) show a significant reduction in the damping coefficients with reduction in Reynolds number, the damping coefficients at the lower Reynolds number being about half the values obtained at the higher Reynolds number. However, the results of a check run made at supersonic speeds at a Reynolds number of about 0.8 million, shown by the flagged symbols in figure 10(b), did not exhibit this reduction in the magnitudes of the damping coefficients.

The reason for there being a large effect of Reynolds number on the damping coefficients at subsonic speeds and little effect at supersonic speeds is not yet understood. Further tests are needed at Reynolds numbers more closely approximating those of full-scale flight in order to clarify this point.

Application of the Results to the Prediction of the Dynamic Behavior of Full-Scale Aircraft

The previous discussion has shown that for the single-degree-of-freedom oscillations studied in the present experiments there exists a range of Mach numbers over which dynamic instability occurs. These results are summarized in figure 15 for the triangular wing-body combination which was investigated at both subsonic and supersonic speeds. For the NACA 0006-63 wing model pivoted at 35 percent M.A.C., it is seen that, for Mach numbers near 0.94 and 1.38, undamped or negatively damped

oscillations occur. Although the evidence is not conclusive due to limitations of the research equipment, the presumption is that negatively damped oscillations will occur over the entire range of Mach numbers between 0.94 and 1.38.

These results, however, are not directly applicable to the prediction of like phenomena for these wings in flight, since in flight an aircraft is free to respond to the impetus of the oscillating lift force. The motion of the airfoil in flight, therefore, consists of a coupled two-degree-of-freedom motion wherein the airfoil experiences vertical translation as well as a pitching motion. In the present experiments, since the center of gravity of the model was fixed, only the pitching motion was experienced by the model.

Some calculations (see appendix C) have been made for the coupled two-degree-of-freedom motion of a tailless aircraft with fixed controls having the same leading-edge sweep as the models of this investigation and with representative full-scale dimensions. Results of these calculations (figs. 16 and 17) indicate that, as expected, the time to damp to one-half amplitude is decreased and the range of Mach numbers in which dynamic instability occurs is reduced, though not eliminated, by consideration of the coupled motion. These calculations have also indicated that the terms containing the stability derivatives C_{L_q} and $C_{L_{\dot{\alpha}}}$ in equation (4) of appendix C are small and may be discarded. This simplification permits the results of this investigation, combined with the results of static wind-tunnel measurements of the lift-curve slope C_{L_α}, to be used to qualitatively predict the dynamic pitching behavior of similar full-scale aircraft.

A comparison of supersonic stability boundary curves for one and two degrees of freedom is shown in figure 17. It is interesting to note that altitude has little effect on the two-degree-of-freedom stability boundary; the magnitude of the reduction of the region of instability is dependent primarily on the inertia-mass ratio of the aircraft and the lift-curve slope C_{L_α}.

While discussing the range of Mach numbers in which unstable oscillations may be expected, it should also be pointed out that the theory of reference 1 indicates that aspect ratio plays a significant roll in determining the damping-in-pitch characteristics of triangular wings at supersonic speeds. According to the theory, the region of supersonic Mach numbers in which negatively damped oscillations may be expected disappears entirely for all center-of-gravity positions when the aspect ratio is reduced to about 2.5 or less, even for the single-degree-of-freedom case. This, incidentally, may account for the fact that no dynamic pitching instability was experienced with the tailless free-flight missile employing a triangular wing swept back 60°, reported in reference 13.

CONCLUSIONS

Results of an experimental investigation of the single degree-of-freedom damping in pitch of two triangular wings having leading edges swept back 45°, with and without a body, made at subsonic speeds in the Ames 12-foot pressure wind tunnel and at supersonic speeds in the Ames 6- by 6-foot supersonic wind tunnel lead to the following conclusions:

1. Theoretical and experimental values of the damping-in-pitch parameter $C_{m_q} + C_{m_{\dot{\alpha}}}$ were in qualitative agreement at both subsonic and supersonic speeds, except for subsonic Mach numbers above 0.94. The dynamic instability, which was observed at subsonic Mach numbers above 0.94, was not predicted by the subsonic theory.

2. The prediction by the supersonic theory of the existence of regions of Mach number and center-of-gravity positions in which negatively damped oscillations may be expected was confirmed by the results of experiments for two axis-of-rotation positions located at 35 percent and 45 percent of the wing mean aerodynamic chord.

3. Considerable improvement in the damping-in-pitch characteristics of a triangular wing can be realized by reducing the span of the wing. Removal of the tips of the wings, which reduced the aspect ratio from 4.0 to 2.67, resulted in a significant reduction in the range of Mach numbers over which negatively damped oscillations were encountered.

4. Calculations made for the two-degree-of-freedom motion which combines the pitching motion studied in the present investigation with a vertical translatory motion shows that, while the additional damping of the oscillation resulting from the translatory motion reduced the range of Mach numbers over which dynamic unstability is experienced, the unstable range was not eliminated.

Ames Aeronautical Laboratory,
National Advisory Committee for Aeronautics,
Moffett Field, Calif.

APPENDIX A

EVALUATION OF THE STABILITY DERIVATIVES C_{m_q} AND $C_{m_{\dot{\alpha}}}$ FOR SUBSONIC SPEEDS

EVALUATION OF C_{m_q}

In the following derivation for the parameter C_{m_q}, the moments about the pitching axis of a thin flat wing in steady pitching flight are assumed to be the same as the moments about an equivalent thin wing in straight flight which has been cambered and twisted to the curvature of the pitching path. The charts and tables in references 6 and 7 can then be used to determine all the necessary characteristics of such a wing except the pitching moment at zero lift due to pitching caused by the effective camber of the wing. This last moment can be approximately evaluated by two-dimensional theory.

The stability derivative C_{m_q} for a pitching axis at a distance $\Delta x_{c.g.}$ ahead of the aerodynamic center is (reference 14)

$$C_{m_q} = C_{m_{q_o}} - C_{L_{q_{a.c.}}} \frac{\Delta x_{c.g.}}{\bar{c}} - 2C_{L_\alpha} \left(\frac{\Delta x_{c.g.}}{\bar{c}} \right)^2 \qquad (A1)$$

where $C_{m_{q_o}}$ is the pitching-moment coefficient due to pitching when the lift due to pitching is zero, and $C_{L_{q_{a.c.}}}$ is the rate of change of lift coefficient with the pitching parameter $q\bar{c}/2V$ for pitching about the aerodynamic center.

For a wing in pitching flight, the path of the wing has a radius of curvature of V/q. The curved flight introduces an angle-of-attack variation along the chord. The resulting moments have been approximately evaluated by assuming a wing in straight flight with a camber and twist such that the angle-of-attack distribution along the chord is the same as that existing on the flat wing in curved flight.

Consider first the pitching moment due to the equivalent camber of the wing when the lift due to pitching is zero. The pitching-moment coefficient at zero lift for a two-dimensional wing section is (reference 15)

$$C_{m_o} = -\frac{\pi}{2}\beta \qquad (A2)$$

where β is defined geometrically also in reference 15. In terms of the triangular wing under consideration

$$\beta = \frac{1}{2}\frac{qc_l}{2V} \tag{A3}$$

where c_l is the local chord. The pitching-moment coefficient due to camber at zero lift for the entire wing can be approximately obtained by integrating the section pitching-moment coefficient

$$C_{m_c} = \frac{2}{S\bar{c}}\int_0^{b/2} \cdot c_l\, C_{m_o}\, c_l\, dy \tag{A4}$$

$$C_{m_c} = \frac{2}{S\bar{c}}\int_0^{b/2} -\frac{\pi}{2}\frac{1}{2}\frac{qc_l}{2V}\, c_l^2 dy = -\frac{9\pi}{32}\frac{q\bar{c}}{2V} \tag{A5}$$

The contribution to C_{m_q} caused by the effective camber becomes, for the triangular wing,

$$(C_{m_q})_c = \frac{\partial C_{m_c}}{\partial(q\bar{c}/2V)} = -\frac{9\pi}{32} \tag{A6}$$

This result should indicate slightly more negative values of $(C_{m_q})_c$ than actually exist because end effects have not been considered, but there should be considerably less error in $(C_{m_q})_c$ than would occur in the lift or pitching-moment coefficient due to angle of attack because at zero lift there are no induced effects of the wake.

The total spanwise twist of the triangular wing due to the pitching motion measured at the three-quarter chord point is

$$\epsilon = -\frac{1}{2}\frac{qc}{2V} = -\frac{3}{4}\frac{q\bar{c}}{2V}$$

The pitching moment due to this twist may be expressed as

$$C_{m_b} = \frac{C_{m_b}}{\epsilon}\epsilon = -\frac{3}{4}\frac{C_{m_b}}{\epsilon}\frac{q\bar{c}}{2V} \tag{A7}$$

The contribution to C_{m_q} caused by the effective spanwise twist of the triangular wing due to the pitching motion becomes then

$$(C_{m_q})_b = \frac{\partial C_{m_b}}{\partial(q\bar{c}/2V)} = -\frac{3}{4}\frac{C_{m_b}}{\epsilon} \tag{A8}$$

where $\frac{C_{m_b}}{\epsilon}$ can be obtained from reference 7. Thus the pitching-moment coefficient due to pitching at zero lift due to pitching becomes, for the triangular wing,

$$C_{m_{q_o}} = (C_{m_q})_c + (C_{m_q})_b = -\frac{9\pi}{32} - \frac{3}{4}\frac{C_{m_b}}{\epsilon} \tag{A9}$$

The lift coefficient due to the pitching motion for rotation about the aerodynamic center is equal to the rate of change of lift coefficient with angle of attack multiplied by the difference between the angle of attack due to the pitching motion and the angle of attack for which the lift due to pitching is zero $(\alpha_r)_o$.

$$C_{L_{a.c.}} = C_{L_\alpha}\,\Delta\alpha \tag{A10}$$

For convenience in using reference 7, the three-quarter-root-chord point was chosen as the reference point to determine $\Delta\alpha$. The effective angle of attack of this point for pitching about $x_{a.c.}$ is

$$2\left(\frac{5}{8} - \frac{x_{a.c.}}{\bar{c}}\right)\frac{q\bar{c}}{2V}$$

where $x_{a.c.}$ is obtained from reference 6. Thus,

$$\Delta\alpha = 2\left(\frac{5}{8} - \frac{x_{a.c.}}{\bar{c}}\right)\frac{q\bar{c}}{2V} - (\alpha_r)_o$$

$$= \frac{q\bar{c}}{2V}\left[2\left(\frac{5}{8} - \frac{x_{a.c.}}{\bar{c}}\right) + \frac{3}{4}\frac{(\alpha_r)_o}{\epsilon}\right] \tag{A11}$$

where $(\alpha_r)_o/\epsilon$ can be obtained from reference 7. Inserting this value

into equation (A10) and taking the derivative with respect to $q\bar{c}/2V$ gives

$$C_{L_{q_{a.c.}}} = \frac{\partial C_{L_{a.c.}}}{\partial(q\bar{c}/2V)} = C_{L_\alpha}\left[2\left(\frac{5}{8} - \frac{x_{a.c.}}{\bar{c}}\right) + \frac{3}{4}\frac{(\alpha_r)_o}{\epsilon}\right] \quad (A12)$$

From equation (A1) then, the stability derivative C_{m_q} for the triangular wing becomes

$$C_{m_q} = -\frac{9\pi}{32} - \frac{3}{4}\frac{C_{m_b}}{\epsilon}\frac{\Delta x_{c.g.}}{\bar{c}}C_{L_\alpha}\left[2\left(\frac{5}{8} - \frac{x_{a.c.}}{\bar{c}}\right) + \frac{3}{4}\frac{(\alpha_r)_o}{\epsilon}\right] - 2C_{L_\alpha}\left(\frac{\Delta x_{c.g.}}{\bar{c}}\right)^2 \quad (A13)$$

where all angles in the above equation are expressed in radians. (Note that C_{m_b}/ϵ and C_{L_α} from references 6 and 7 must be converted to radians before inserting in equation (A13).)

The effects of compressibility can be approximately considered by calculating C_{m_q} in incompressible flow for a triangular wing, the aspect ratio of which has been reduced by the compressibility factor $\sqrt{1-M^2}$ and multiplying the value of C_{m_q} obtained by $\frac{1}{\sqrt{1-M^2}}$.

EVALUATION OF $C_{m_{\dot{\alpha}}}$

The stability derivative $C_{m_{\dot{\alpha}}}$ can be approximately evaluated from operational expressions for the lift on a finite wing, the angle of attack of which varies with the distance traveled. Using the nomenclature of reference 8, a sinusoidal variation of angle of attack is written as

$$\alpha = Ae^{ins} \quad (A14)$$

where

A amplitude of the oscillation

s distance traveled in half mean aerodynamic chord lengths

n 2π times the number of cycles per half mean aerodynamic chord length of travel

The lift coefficient resulting from this angle-of-attack variation is

$$C_L(s) = \bar{C}_{L_1}(D)\, Ae^{ins} \tag{A15}$$

where $\bar{C}_{L_1}(D)$ is the operational form of the indicial lift coefficient, the response of the wing to a sudden unit change of angle of attack. Solutions have been evaluated in reference 8 as

$$C_{L_n}(s) = \bar{C}_{L_1}(in)\, Ae^{ins} \tag{A16}$$

$$C_{L_n}(s) = 2\pi\,[F(n) + iG(n)]\, Ae^{ins} \tag{A17}$$

where values of $F(n)$ and $G(n)$ have been determined for elliptic wings of aspect ratios 3 and 6. In addition, as pointed out in reference 8, the center of pressure of the unsteady lift for a wing of infinite aspect ratio remains on the quarter chord throughout the motion.

It is assumed that the unsteady lift on the triangular wing of this report would be equal to that for an elliptic wing of the same aspect ratio. Also, from the results of the infinite aspect ratio calculation, it is assumed that the center of pressure for unsteady lift is the same as for steady lift. The moment about the pitching axis of the wing due to a sinusoidal change of angle of attack can then be expressed as

$$M = -\frac{1}{2}\rho V^2 S\, \Delta x_{c.g.}\, C_{L_n}(s) \tag{A18}$$

This same moment can also be expressed in differential form as a moment due to α and a moment due to $\dot{\alpha}$

$$M = \frac{\partial M}{\partial \dot{\alpha}}\,\dot{\alpha} + \frac{\partial M}{\partial \alpha}\,\alpha \tag{A19}$$

Thus,

$$(\partial M/\partial \dot{\alpha})\,\dot{\alpha} + (\partial M/\partial \alpha)\,\alpha = -\frac{1}{2}\rho V^2 S\, \Delta x_{c.g.} C_{L_n}(s)$$

Since

$$e^{ins} = e^{i\omega t} \tag{A20}$$

on making this substitution,

$$\frac{\partial M}{\partial \dot{\alpha}} i\omega A e^{i\omega t} + \frac{\partial M}{\partial \alpha} A e^{i\omega t} = -\frac{1}{2}\rho V^2 S \, \Delta x_{c.g.} \, 2\pi \, [F(n) + iG(n)] \, A e^{i\omega t} \tag{A21}$$

Separating the imaginary terms from the real terms and canceling $Ae^{i\omega t}$

$$i\omega \frac{\partial M}{\partial \dot{\alpha}} = -\frac{1}{2}\rho V^2 S \, \Delta x_{c.g.} \, i2\pi \, G(n) \tag{A22}$$

In reference 16, the function $2\pi \, G(n)$ is given as

$$2\pi \, G(n) = -C_1 \frac{r_1 n}{r_1^2 + n^2} - C_2 \frac{r_2 n}{r_2^2 + n^2} \tag{A23}$$

where C_1, C_2, r_1, and r_2 are constants which depend on aspect ratio. Interpolating between values of the constants for the examples of aspect ratios 3 and 6 in reference 16, the values for an aspect ratio of 4 become approximately

$$C_1 = -1.50$$

$$r_1 = -0.36$$

$$r_2 = C_2 = 0$$

and

$$C_{m_{\dot{\alpha}}} = \frac{\partial M/\partial \dot{\alpha}}{\frac{1}{4}\rho V S \bar{c}^2} = \frac{\Delta x_{c.g.}}{\bar{c}} \left(\frac{2V}{\omega \bar{c}} \right) \frac{(1.5)(0.36)\, n}{(0.36)^2 + n^2} \tag{A24}$$

But since

$$n = \frac{\omega \bar{c}}{2V} << 0.36 \tag{A25}$$

the value of $C_{m_{\dot{\alpha}}}$ for the range of frequencies of interest in this discussion becomes simply

$$C_{m_{\dot{\alpha}}} \approx 4 \frac{\Delta x_{c.g.}}{\bar{c}} \tag{A26}$$

for a wing of aspect ratio 4. Due to the many approximations involved in this derivation, a high degree of refinement in computing the effects of compressibility is not justified. The values of $C_{m_{\dot{\alpha}}}$ at the higher subsonic Mach numbers were obtained by multiplying equation (A26) by $\frac{1}{\sqrt{1-M^2}}$.

APPENDIX B

DERIVATION OF THE DAMPING IN PITCH OF A SLENDER BODY

In the development given below, the method used by Ribner in reference 11 to obtain the stability derivatives of low-aspect-ratio triangular wings is followed to obtain the damping-in-pitch derivatives of a slender body of revolution.

Consider the body moving with velocity V and angle of attack α, as shown in the sketch below:

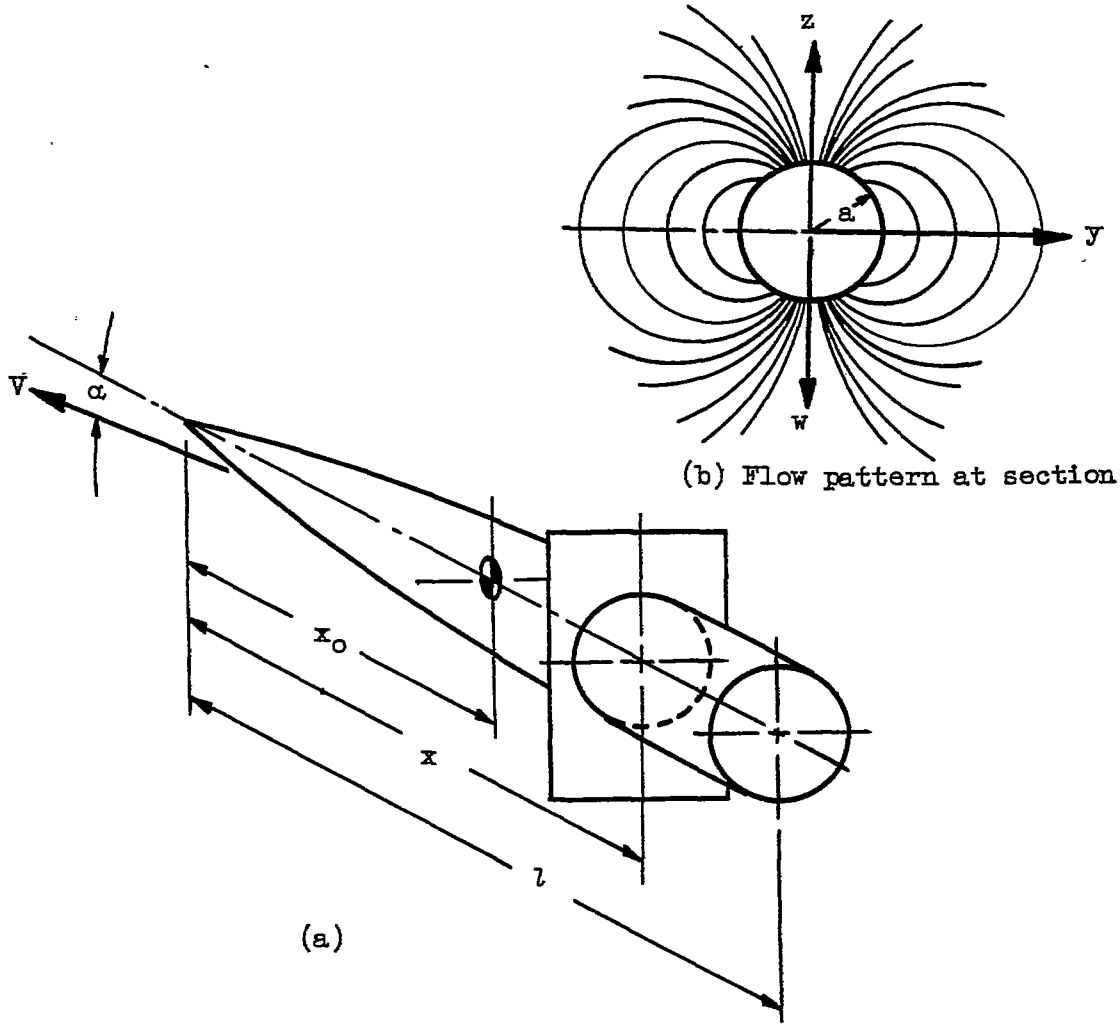

(b) Flow pattern at section

The linearized potential equation for unsteady flow is written as

$$B^2 \frac{\partial^2 \varphi}{\partial x^2} - \frac{\partial^2 \varphi}{\partial y^2} - \frac{\partial^2 \varphi}{\partial z^2} + \frac{2V}{a^2} \frac{\partial^2 \varphi}{\partial x \partial t} + \frac{1}{a^2} \frac{\partial^2 \varphi}{\partial t^2} = 0 \tag{B1}$$

where the coordinate system is moving in the negative x direction with the velocity V. If the development is limited in application to a slender body performing slow oscillations, $\partial^2\varphi/\partial x^2$, $\partial^2\varphi/\partial t^2$, and $\partial^2\varphi/\partial x \partial t$ may be considered to be negligible. Equation (B1) thus reduces to

$$\frac{\partial^2 \varphi}{\partial y^2} + \frac{\partial^2 \varphi}{\partial z^2} = 0 \tag{B2}$$

Physically, equation (B2) implies that the flow at any transverse cross section of the body is similar to a two-dimensional flow. The flow at any section may thus be expressed as the potential flow for a circular lamina moving downward in its own plane with a velocity αV (see sketch, page 29). For this case, the potential is equivalent to that of a doublet with its axis parallel to the z axis (reference 10) so that

$$\varphi = \frac{wa^2 z}{y^2+z^2} \tag{B3}$$

where

a body radius at a section a distance x from the nose

w vertical velocity of the section

It can be shown that equation (B3) is a solution of equation (B2). The local loading is

$$\Delta p = 2\rho \left(\frac{\partial \varphi}{\partial t} + V \frac{\partial \varphi}{\partial x} \right) \tag{B4}$$

The pitching-moment coefficient due to the rate of change of angle of attack with time $C_{m_{\dot{\alpha}}}$ arises from the term $2\rho \frac{\partial \varphi}{\partial t}$; the term $2\rho \frac{\partial \varphi}{\partial x}$ yields the pitching-moment coefficient due to steady pitching C_{m_q}.

EVALUATION OF $C_{m_{\dot{\alpha}}}$

As mentioned previously, for an accelerated translatory motion, the contribution to the local loading is given by the term

$$\Delta p = 2\rho \frac{\partial \varphi}{\partial t} = 2\rho \frac{\partial \varphi}{\partial \alpha} \dot{\alpha} \tag{B5}$$

From equation (B3), since $w = \alpha V$,

$$\frac{\partial \varphi}{\partial \alpha} = Va^2 \frac{z}{y^2+z^2}$$

On the surface of the body

$$y^2 + z^2 = a^2$$

Therefore,

$$\Delta p = 2\rho V \dot{\alpha} z = 2\rho V \dot{\alpha} \sqrt{a^2-y^2} \tag{B6}$$

The pitching moment of the local loading about an axis a distance x_o from the nose may be written,

$$\left.\begin{aligned} M_x &= -\int_{-a}^{a} (x-x_o)\, \Delta p\, dy \\ &= -\rho V \dot{\alpha}\, (x-x_o)\, \pi a^2 \end{aligned}\right\} \tag{B7}$$

The total pitching moment due to $\dot{\alpha}$ may then be found by the integration of equation (B7) over the body length

$$M = -\rho V \dot{\alpha} \int_o^l \pi a^2 (x-x_o)\, dx \tag{B8}$$

The term $\int_o^l \pi a^2 dx$ gives the body volume, while $\int_o^l \pi a^2 x dx$ expresses

the moment of the body volume about the nose. If the volume is written as $B_m l$, where B_m is the mean body cross-sectional area, the pitching moment can be written as

$$M = -\rho V \dot{\alpha} \left(\bar{x} B_m l - B_m l x_o\right) = -\rho V \dot{\alpha} B_m l \left(\bar{x} - x_o\right) \tag{B9}$$

where $\bar{x}$ is the distance of the centroid of the body volume from the nose. Then, referring the pitching moment to the wing dimensions, the moment in coefficient form is

$$C_m = -\frac{2\dot{\alpha}}{V} \frac{B_m l}{Sc} \left(\bar{x} - x_o\right) \tag{B10}$$

The stability derivative is formed by the derivative of C_m with respect to $\dot{\alpha}\bar{c}/2V$. It is

$$C_{m_{\dot{\alpha}}} = -\frac{4 B_m l}{S\bar{c}^2} \left(\bar{x} - x_o\right) \tag{B11}$$

EVALUATION OF C_{m_q}

For an angular pitching velocity q about an axis located at a distance x_o from the nose, the vertical velocity of a station on the body located at x is

$$w = q(x - x_o) \tag{B12}$$

Then

$$\varphi = a^2 q (x - x_o) \frac{z}{y^2 + z^2} \tag{B13}$$

From (B4), the local loading term is

$$\Delta p = 2\rho V \frac{\partial \varphi}{\partial x} \tag{B14}$$

Performing the indicated differentiation, there results for the local loading on the surface of the body

$$\Delta p = 4q\rho V \left(\frac{x - x_o}{a}\right) \frac{da}{dx} z + 2q\rho V z \tag{B15}$$

The pitching moment of the local loading is again

$$M_x = -2\int_o^a \Delta p\,(x-x_o)\,dy$$

$$= -8q\rho V\int_o^a \frac{(x-x_o)^2}{a}\frac{da}{dx}\sqrt{a^2-y^2}\,dy - 4q\rho V\int_o^a (x-x_o)\sqrt{a^2-y^2}\,dy$$

$$= 2\pi q\rho V\,(x-x_o)^2\,a\frac{da}{dx} - q\rho V\pi a^2\,(x-x_o) \qquad (B16)$$

The total pitching moment due to q is

$$M = \int_o^l M_x dx = -q\rho V\int_o^l 2\pi a\frac{da}{dx}(x-x_o)^2\,dx - q\rho V\int_o^l \pi a^2\,(x-x_o)\,dx \qquad (B17)$$

The quantity $2\pi a\frac{da}{dx}$ expresses the variation of the cross-sectional area of the body with x, or is dB/dx. Since the body cross-sectional area is zero at $x = 0$, and is equal to the area of the body base at $x = l$, the first integral in equation (B17) reduces to

$$-q\rho VB_b\,(l-x_o)^2 + 2\rho qV\int_o^l \pi a^2\,(x-x_o)\,dx$$

The pitching moment may then be written

$$M = -q\rho VB_b\,(l-x_o)^2 + q\rho VB_m l\,(\bar{x}-x_o) \qquad (B18)$$

Reducing to coefficient form in terms of the wing dimensions,

$$C_m = -\frac{2qB_b}{VS\bar{c}}(l-x_o)^2 + \frac{2qlB_m}{VS\bar{c}}(\bar{x}-x_o) \qquad (B19)$$

and forming the stability derivative, $\frac{\partial C_m}{\partial(q\bar{c}/2V)}$,

$$C_{m_q} = -\frac{4B_b}{Sc^2}(l-x_o)^2 + \frac{4B_m l}{Sc^2}(\bar{x}-x_o) \qquad (B20)$$

The total damping in pitch of the body is the sum of C_{m_q} and $C_{m_{\dot{\alpha}}}$. It thus appears upon adding equations (B20) and (B11) that

$$C_{m_q} + C_{m_{\dot{\alpha}}} = -\frac{4B_b}{Sc^2}(l-x_o)^2 \qquad (B21)$$

APPENDIX C

THE DAMPING OF THE SHORT-PERIOD PITCHING OSCILLATIONS OF A WING HAVING TWO DEGREES OF FREEDOM

In the following analysis, it is assumed that changes in the forward speed of the aircraft are negligible. The assumption effectively limits the development to one describing the character of the short-period pitching oscillations of the aircraft.

Consider the case of a triangular wing aircraft in steady flight. If the aircraft is displaced from its state of equilibrium, the resulting equations of longitudinal motion (in wind-axis notation) are:

$$\left.\begin{aligned} &\text{(a)}\quad \tfrac{1}{2}\rho V^2 S\left(C_{L_\alpha}\alpha + \frac{\dot{\alpha}\bar{c}}{2V}C_{L_{\dot{\alpha}}} + \frac{q\bar{c}}{2V}C_{L_q}\right) = mV\frac{d\gamma}{dt} \\ &\text{(b)}\quad \tfrac{1}{2}\rho V^2 S\bar{c}\left(C_{m_\alpha}\alpha + \frac{\dot{\alpha}\bar{c}}{2V}C_{m_{\dot{\alpha}}} + \frac{q\bar{c}}{2V}C_{m_q}\right) = I\frac{d^2\theta}{dt^2} \end{aligned}\right\} \quad \text{(C1)}$$

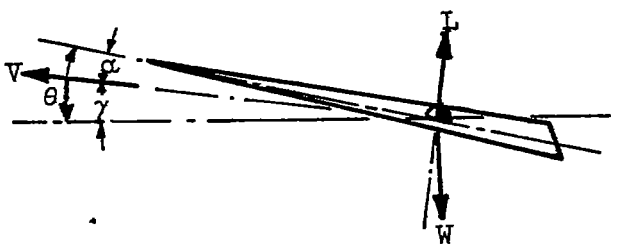

From the sketch above, $\theta = \alpha + \gamma$, so that $q = \frac{d\theta}{dt} = \frac{d\alpha}{dt} + \frac{d\gamma}{dt}$ and $\frac{dq}{dt} = \frac{d^2\theta}{dt^2}$.

Making the above substitutions and converting to operational notation,

$$\left.\begin{aligned} &\text{(a)}\quad \left[\left(\frac{\bar{c}}{2V}C_{L_{\dot{\alpha}}} + 2\tau\right)D + C_{L_\alpha}\right]\alpha + \left(\frac{\bar{c}}{2V}C_{L_q} - 2\tau\right)q = 0 \\ &\text{(b)}\quad \left(\frac{\bar{c}}{2V}C_{m_{\dot{\alpha}}}D + C_{m_\alpha}\right)\alpha + \left(\frac{\bar{c}}{2V}C_{m_q} - kD\right)q = 0 \end{aligned}\right\} \quad \text{(C2)}$$

where $\tau = m/\rho VS$, $k = 2I/\rho V^2 S\bar{c}$, $D = d/dt$.

Solving the above equations simultaneously gives

$$\left\{D^2\left[-k\left(\frac{\bar{c}}{2V}C_{L_{\dot{\alpha}}}+2\tau\right)\right]+D\left[\left(\frac{\bar{c}}{2V}\right)^2\left(C_{m_q}C_{L_{\dot{\alpha}}}-C_{m_{\dot{\alpha}}}C_{L_q}\right)+\right.\right.$$

$$\left.\left.\frac{\tau\bar{c}}{V}\left(C_{m_q}+C_{m_{\dot{\alpha}}}\right)-kC_{L_\alpha}\right]+\left[\frac{\bar{c}}{2V}\left(C_{m_q}C_{L_\alpha}-C_{m_\alpha}C_{L_q}\right)+2\tau C_{m_\alpha}\right]\right\}\alpha \text{ or } q = 0 \tag{C3}$$

Equation (C3) is recognized as the characteristic equation of free vibrations with viscous damping (reference 17), the solution of which shows that the magnitude of the oscillations will build up or die out according to whether the term ψ below is positive or negative.

$$\psi = \frac{\frac{\tau\bar{c}}{V}\left(C_{m_{\dot{\alpha}}}+C_{m_q}\right)+\left(\frac{\bar{c}}{2V}\right)^2\left(C_{m_q}C_{L_{\dot{\alpha}}}-C_{m_{\dot{\alpha}}}C_{L_q}\right)-kC_{L_\alpha}}{2k\left(\frac{\bar{c}}{2V}C_{L_{\dot{\alpha}}}+2\tau\right)} \tag{C4}$$

The stability boundary curve for the two-degree-of-freedom motion may thus be obtained by setting the expression for ψ in equation (C4) equal to zero, and replacing the stability derivative terms therein with the general forms given below:

$$\left.\begin{aligned}
&\text{(a)}\quad C_{m_q} = C_{m_{q_o}} - \left(\frac{\Delta x_{c.g.}}{\bar{c}}\right)C_{L_{q_o}} - 2\left(\frac{\Delta x_{c.g.}}{\bar{c}}\right)^2 C_{L_\alpha}\\
&\text{(b)}\quad C_{m_{\dot{\alpha}}} = C_{m_{\dot{\alpha}_o}} - \left(\frac{\Delta x_{c.g.}}{\bar{c}}\right)C_{L_{\dot{\alpha}}}\\
&\text{(c)}\quad C_{L_q} = C_{L_{q_o}} + 2\left(\frac{\Delta x_{c.g.}}{\bar{c}}\right)C_{L_\alpha}
\end{aligned}\right\} \tag{C5}$$

where the subscripted terms are referred to the lateral axis passing through the aerodynamic center of the triangular wing, and the value $\left(\frac{\Delta x_{c.g.}}{\bar{c}}\right)$ represents the distance of the center of gravity from the aerodynamic center, measured positive forward of the aerodynamic center. The stability derivatives which appear in the above equations may be computed for supersonic speeds from results given in reference 1.

Performing the manipulations indicated above, there again results a quadratic equation for $\left(\frac{\Delta x_{c.g.}}{\bar{c}}\right)$ of the form

$$\left(\frac{\Delta x_{c.g.}}{\bar{c}}\right) = -\frac{b}{2a} \pm \sqrt{\left(\frac{b}{2a}\right)^2 - \frac{c}{a}} \tag{C6}$$

where

$$a = \frac{2m}{\rho S \bar{c}} C_{L_\alpha}$$

$$b = \frac{m}{\rho S \bar{c}} \left(C_{L_{q_o}} + C_{L_{\dot{\alpha}}}\right) + \frac{1}{2} C_{L_\alpha} C_{m_{\dot{\alpha}_o}}$$

$$c = -\frac{m}{\rho S \bar{c}} \left(C_{m_{q_o}} + C_{m_{\dot{\alpha}_o}}\right) + \frac{1}{4} \left(C_{L_{q_o}} C_{m_{\dot{\alpha}_o}} - C_{m_{q_o}} C_{L_{\dot{\alpha}}}\right) + \frac{2I}{\rho S \bar{c}^3} C_{L_\alpha}$$

The time to damp to one-half amplitude for the wing oscillating about a given center-of-gravity position is obtained by computing ψ for that position, and substituting in the expression

$$T_{1/2} = -\frac{0.693}{\psi}$$

REFERENCES

1. Ribner, Herbert S., and Malvestuto, Frank S., Jr.: Stability Derivatives of Triangular Wings at Supersonic Speeds. NACA Rep. 908, 1948.

2. Miles, John W.: On Damping in Pitch for Delta Wings. Jour. Aero. Sci., vol. 16, no. 9, Sept. 1949, p. 574.

3. Frick, Charles W., and Olson, Robert N.: Flow Studies in the Asymmetric Adjustable Nozzle of the Ames 6- by 6-Foot Supersonic Wind Tunnel. NACA RM A9E24, 1949.

4. Lindsey, W. F., Daley, Bernard N., and Humphreys, Milton D.: The Flow and Force Characteristics of Supersonic Airfoils at High Subsonic Speeds. NACA TN 1211, 1947.

5. Haack, W.: Geschossformen kleinsten Wellenwiderstandes. Bericht 139, Teil I der Lilienthal Gesselschaft für Luftfahrtforschung, pp. 14-28, 1941.

6. DeYoung, John: Theoretical Additional Span Loading Characteristics of Wings With Arbitrary Sweep, Aspect Ratio, and Taper Ratio. NACA TN 1491, 1947.

7. Stevens, Victor I.: Theoretical Basic Span Loading Characteristics of Wings With Arbitrary Sweep, Aspect Ratio, and Taper Ratio. NACA TN 1772, 1948.

8. Jones, Robert T.: The Unsteady Lift of a Wing of Finite Aspect Ratio. NACA Rep. 681, 1940.

9. Malvestuto, Frank S., Jr., and Margolis, Kenneth: Theoretical Stability Derivatives of Thin Swept-Back Wings Tapered to a Point With Swept-Back or Swept-Forward Trailing Edges for a Limited Range of Supersonic Speeds. NACA Rep. 971, 1949.

10. Munk, Max M.: The Aerodynamic Forces on Airship Hulls. NACA Rep. 184, 1924.

11. Ribner, Herbert S.: The Stability Derivatives of Low-Aspect-Ratio Triangular Wings at Subsonic and Supersonic Speeds. NACA TN 1423, 1947.

12. Miles, John W.: Unsteady Flow Theory in Dynamic Stability. Jour. Aero. Sci., vol. 17, no. 1, Jan. 1950, pp. 62-63.

13. Mitcham, Grady L., Stevens, Joseph E., and Norris, Harry P.: Aerodynamic Characteristics and Flying Qualities of a Tailless Triangular-Wing Airplane Configuration as Obtained From Flights of Rocket-Propelled Models at Transonic and Low Supersonic Speeds. NACA RM L9L07, 1950.

14. Cotter, William E., Jr.: Summary and Analysis of Data on Damping in Yaw and Pitch for a Number of Airplane Models. NACA TN 1080. 1946.

15. Glauert, H.: The Elements of Aerofoil and Airscrew Theory. The MacMillan Company, New York, 1943, p. 86.

16. Jones, Robert T.: The Unsteady Lift of a Finite Wing. NACA TN 682, 1939.

17. Myklestad, N. O.: Vibration Analysis. McGraw-Hill Book Company, New York, 1944.

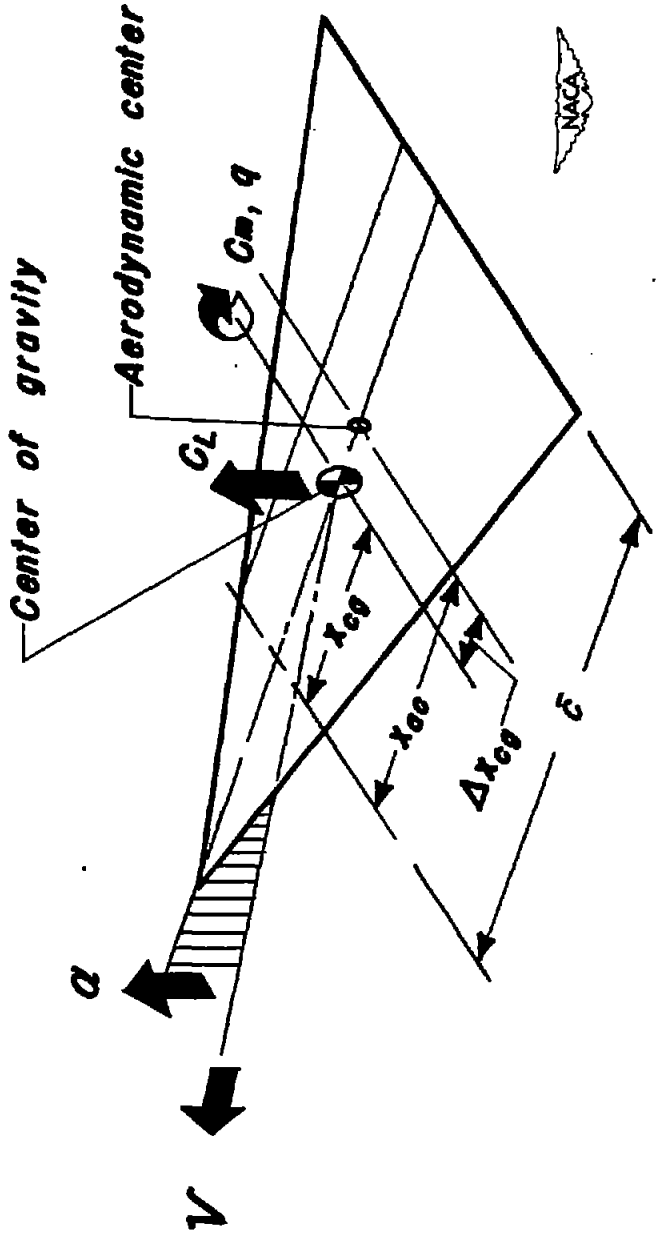

Figure 1.- Velocities, forces, and moments relative to stability axes with origin at the center of gravity.

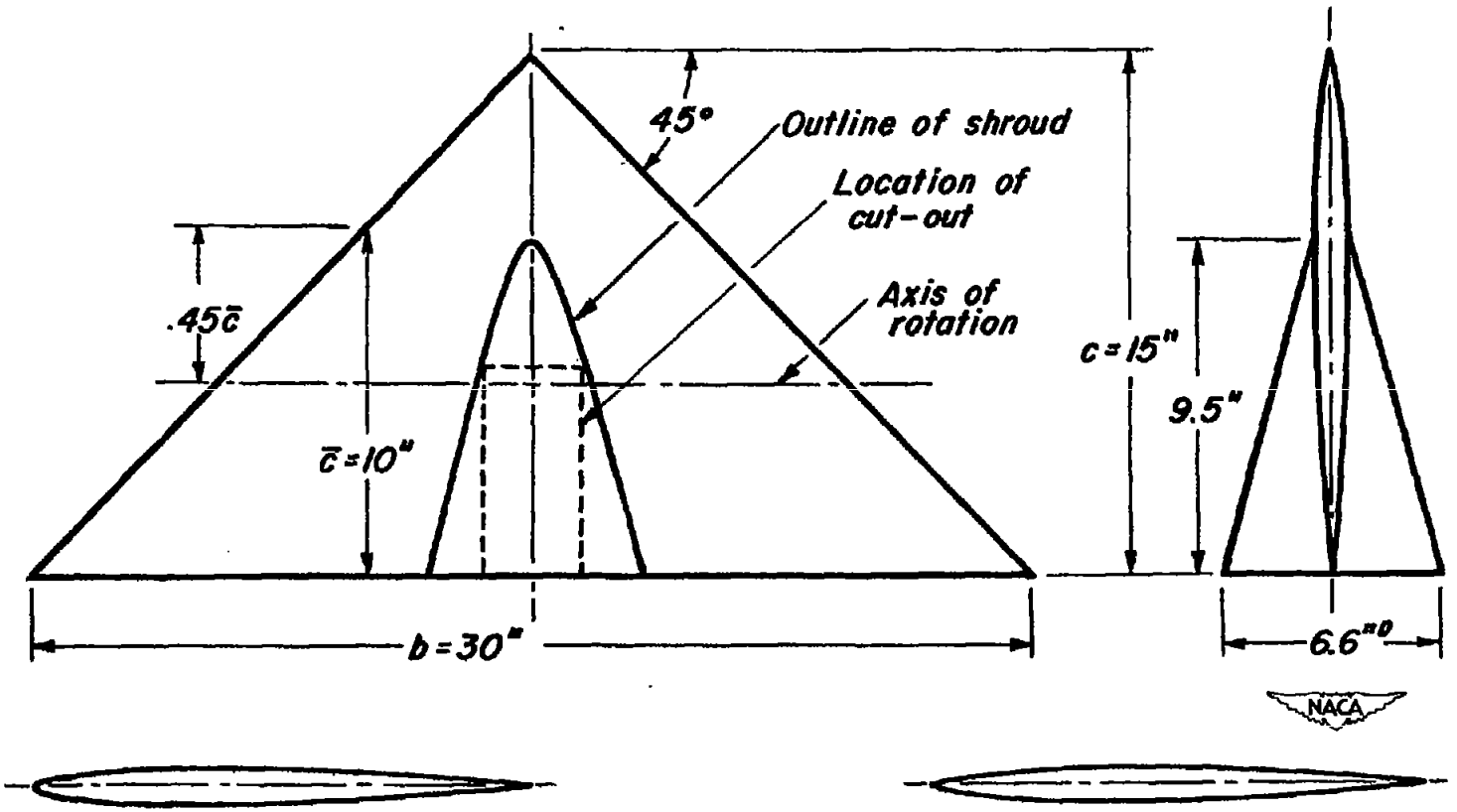

Round leading-edge section, NACA 0006-63

Sharp leading-edge section

Figure 2.- Model with shroud attached, and the two airfoil sections investigated.

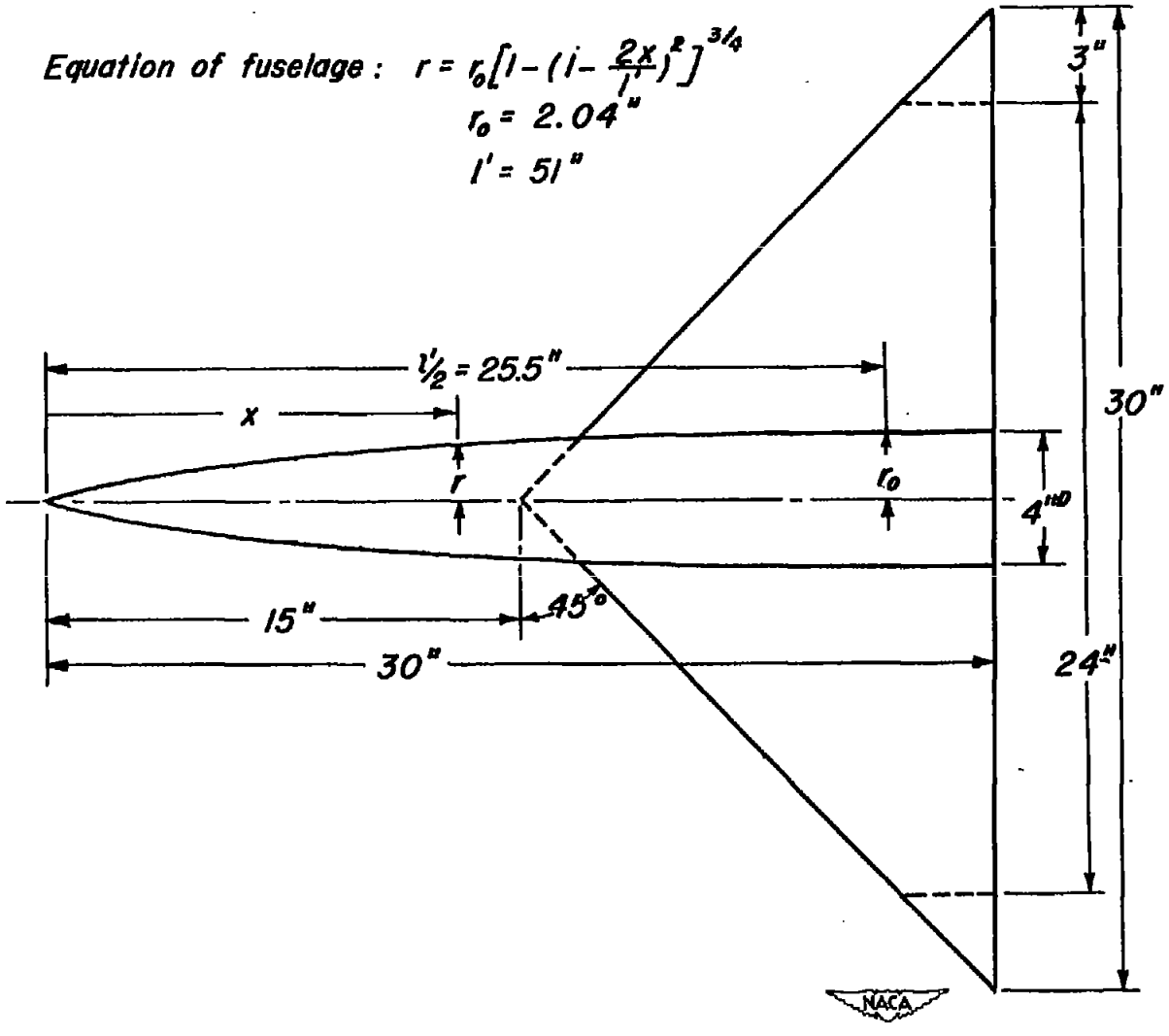

Figure 3.– Sketch of model with fuselage attached, showing spanwise station at which tips were removed.

Figure 4.– The triangular wing–body combination mounted in the Ames 6– by 6–foot supersonic wind tunnel.

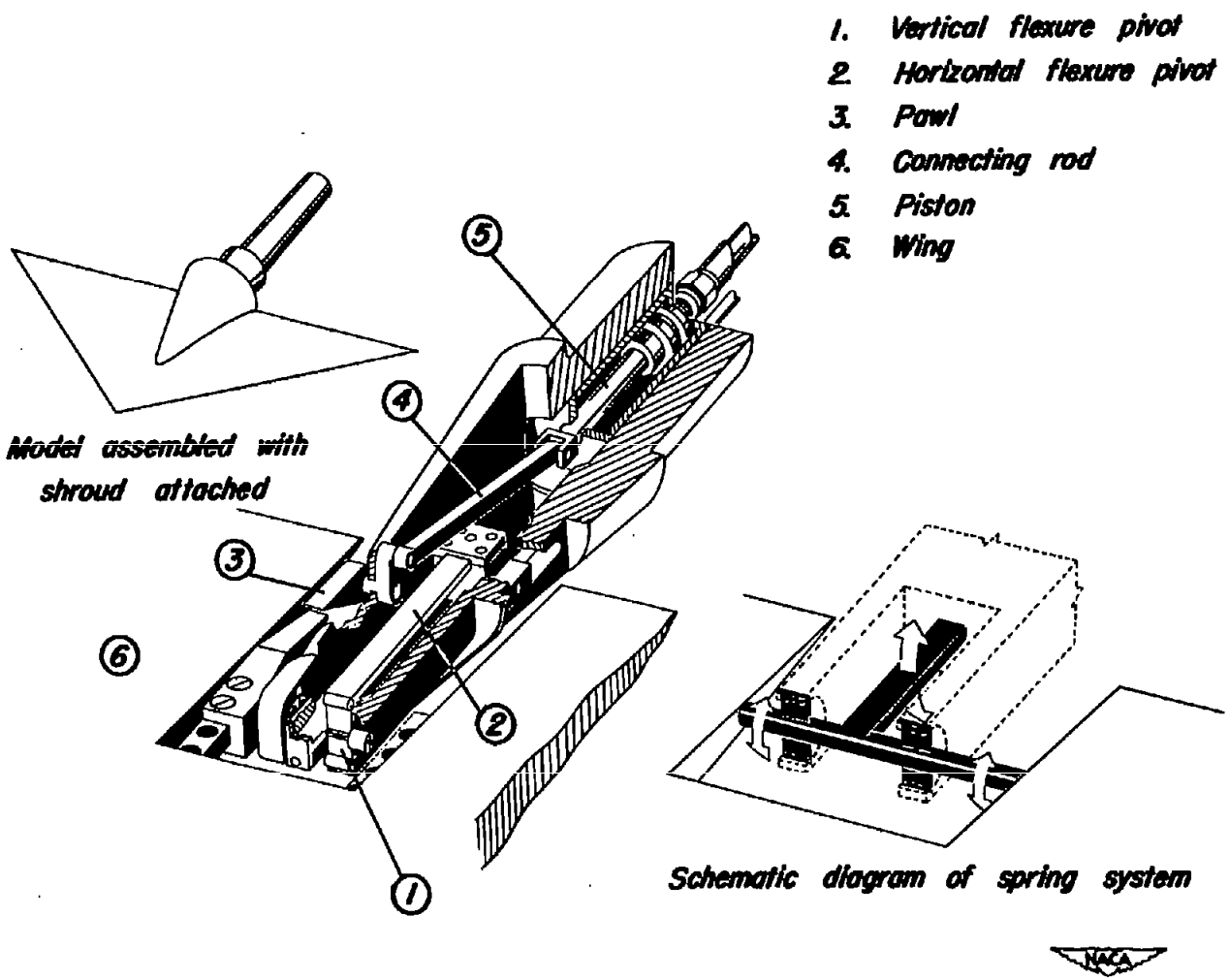

Figure 5.- Spring support system for oscillating airfoil tests.

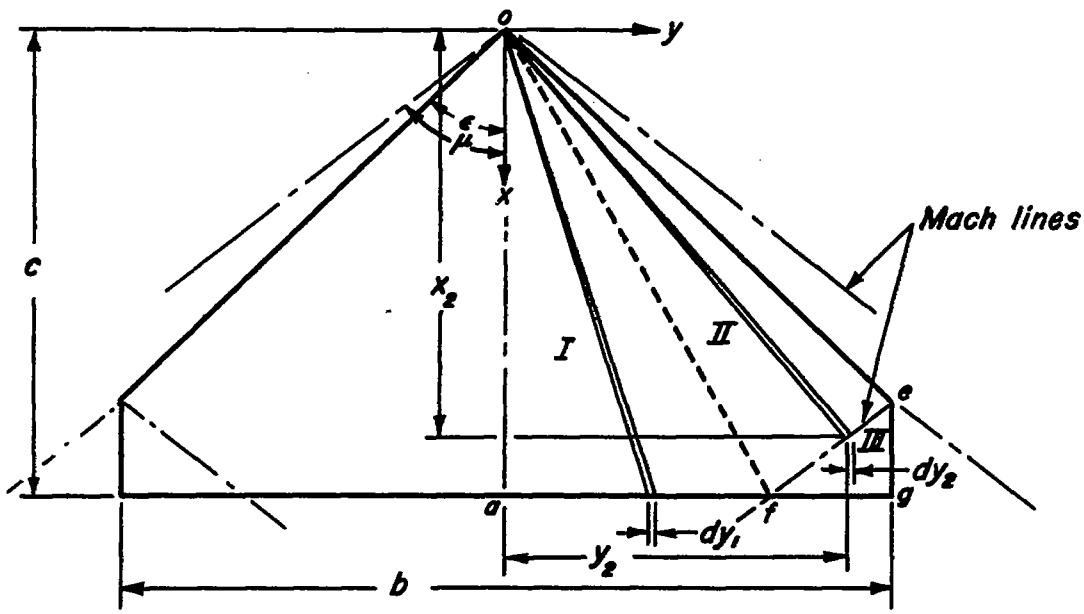

Areas of integration:

Sector I (oaf) $dS = \frac{1}{2} c\, dy_1 = \frac{1}{2} c^2 C d\eta$; $\eta = 0$ to $\eta = \eta_1$

Sector II (ofe) $dS = \frac{1}{2} x_2\, dy_2 = \frac{1}{2}\left[\frac{b(m+1)}{2C(1+m\eta)}\right]^2 C d\eta$; $\eta = \eta_1$ to $\eta = 1$.

$$\eta = \frac{y}{xC}, \quad \eta_1 = \frac{b(m+1)-2cC}{2mcC}, \quad C = \tan\epsilon, \quad m = \frac{\tan\epsilon}{\tan\mu}$$

Figure 6.— Areas of integration for obtaining theoretical pitching stability derivatives at supersonic speeds for triangular wings with cut-off tips.

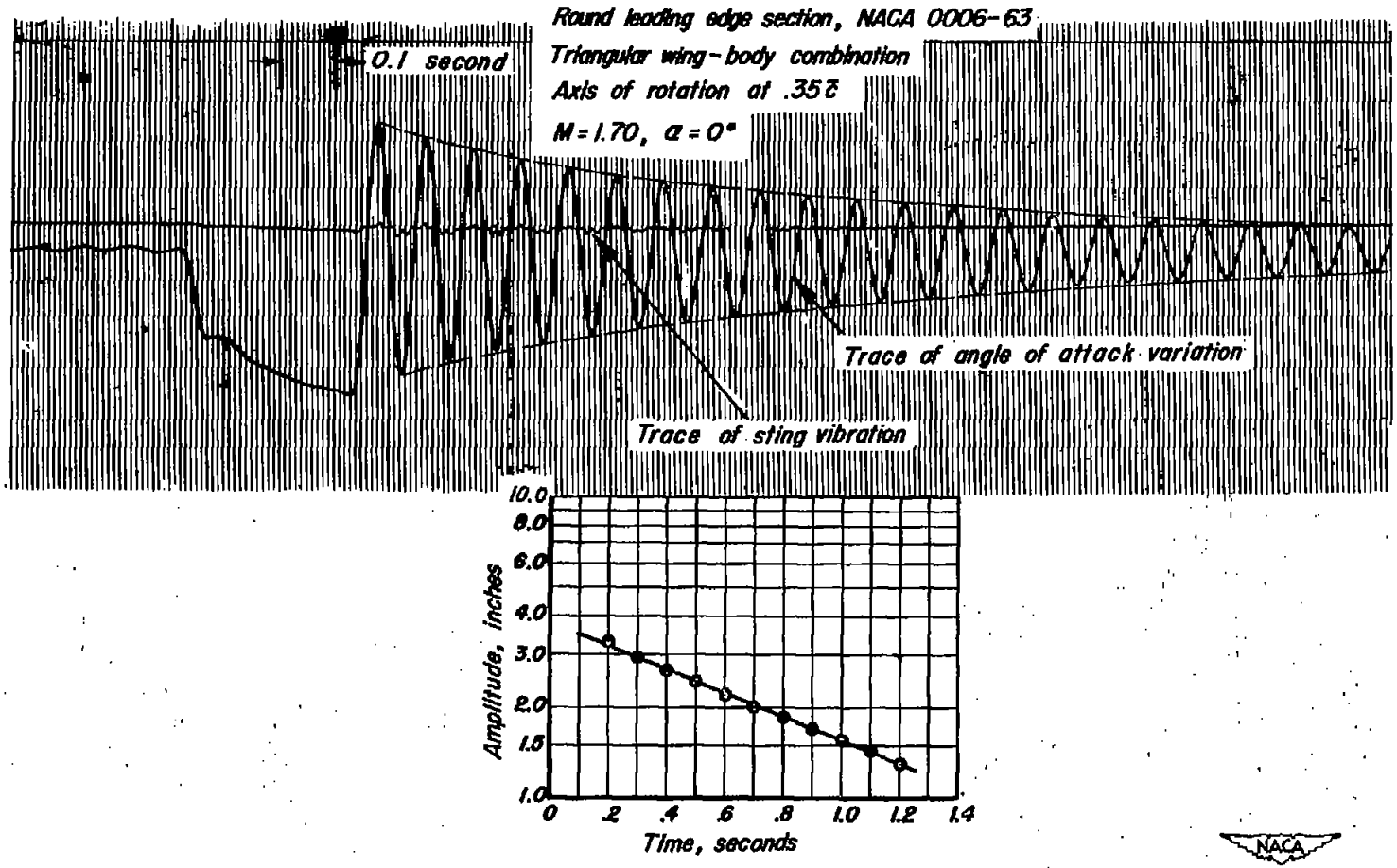

Figure 7.- Reproduction of a typical oscillograph record and its semilogarithmic reduction.

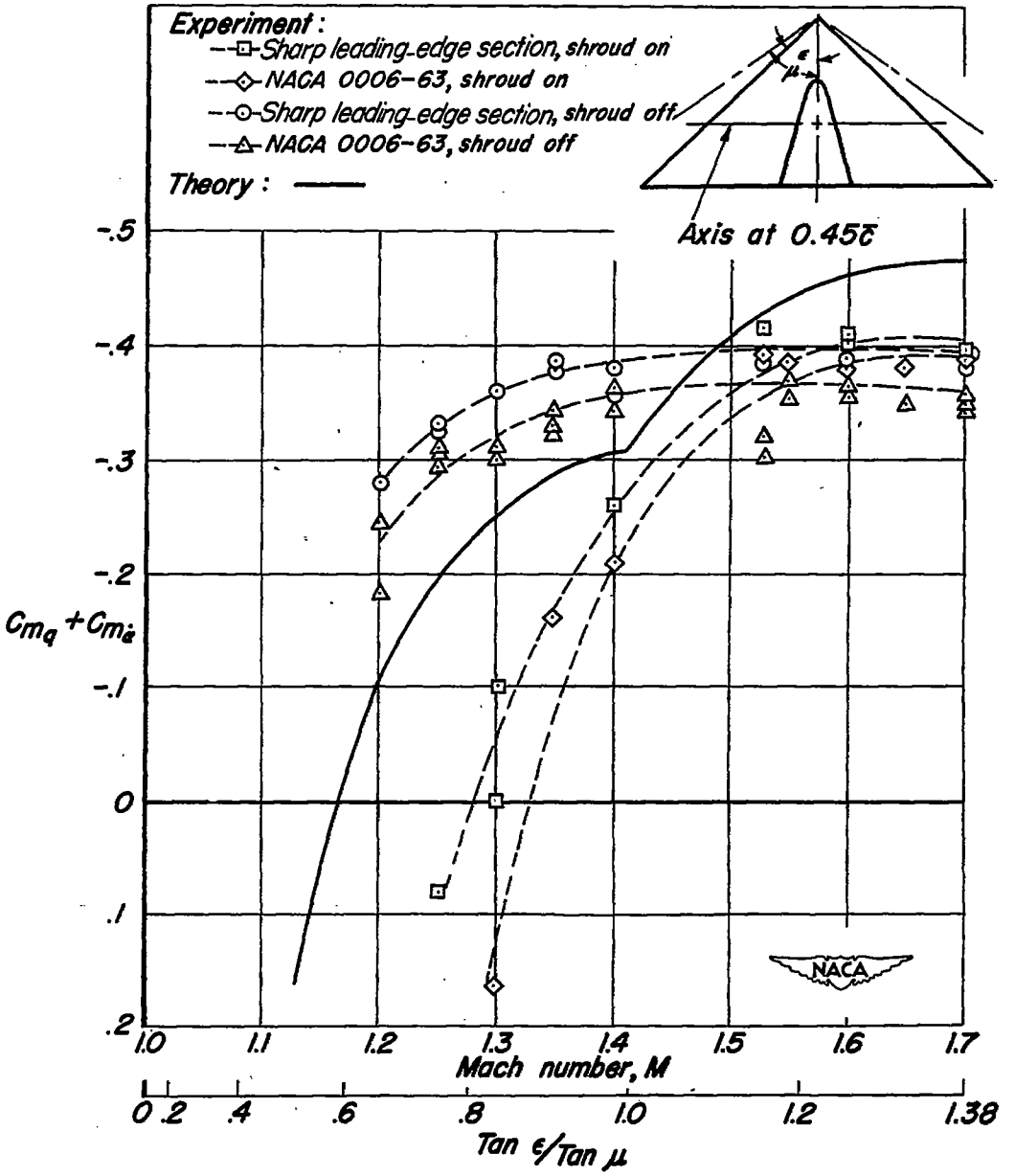

(a) $\alpha = 0°$

Figure 8. - Experimental damping in pitch coefficients for the triangular wing with shroud on and off at $\alpha = 0°$ and 5° and axis of rotation at $0.45\bar{c}$.

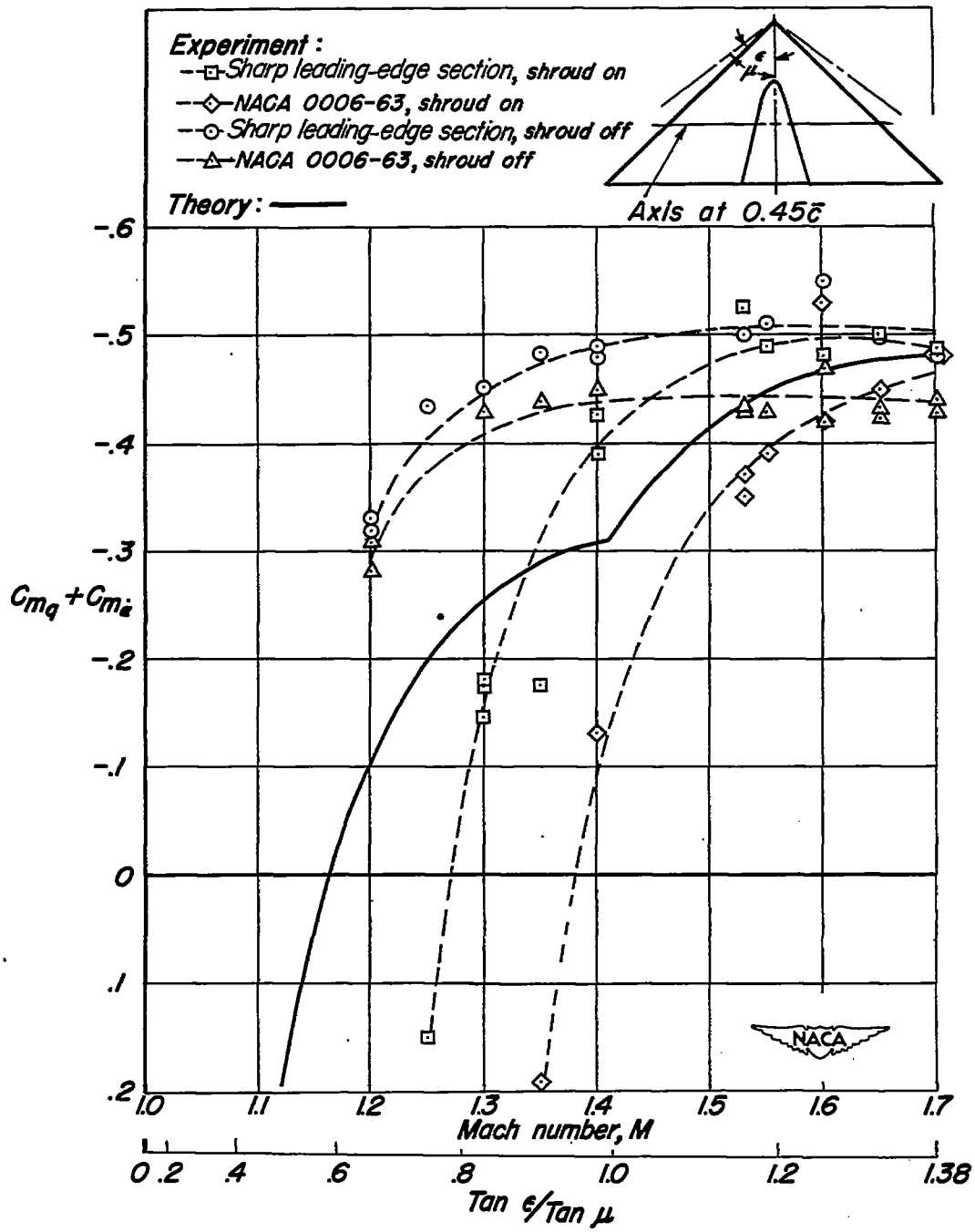

(b) $\alpha = 5°$

Figure 8. - Concluded.

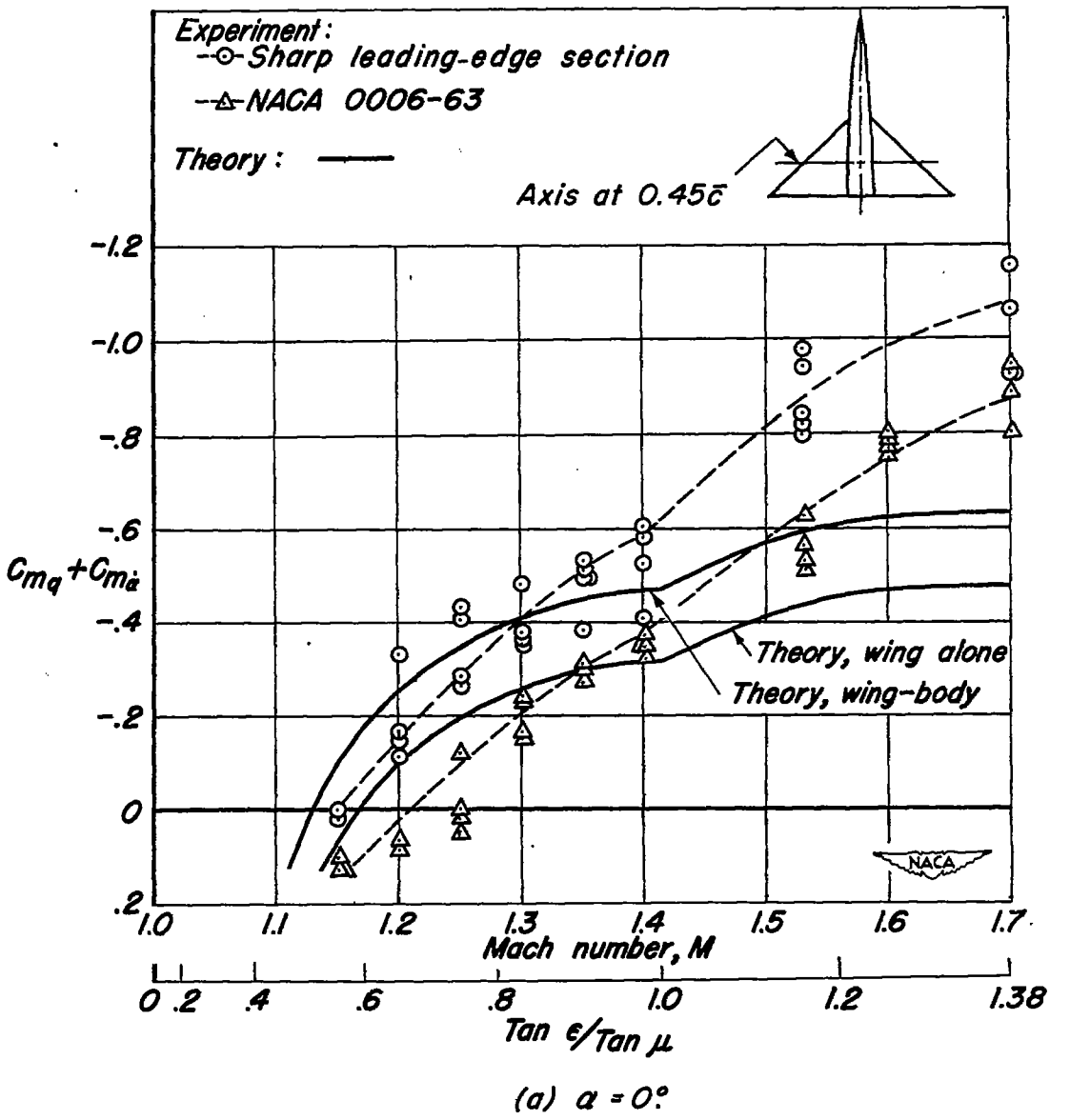

(a) $\alpha = 0°$

Figure 9. - Experimental damping in pitch coefficients for the triangular wing-body combination at $\alpha = 0°$ and 5° and axis of rotation at 0.45c̄.

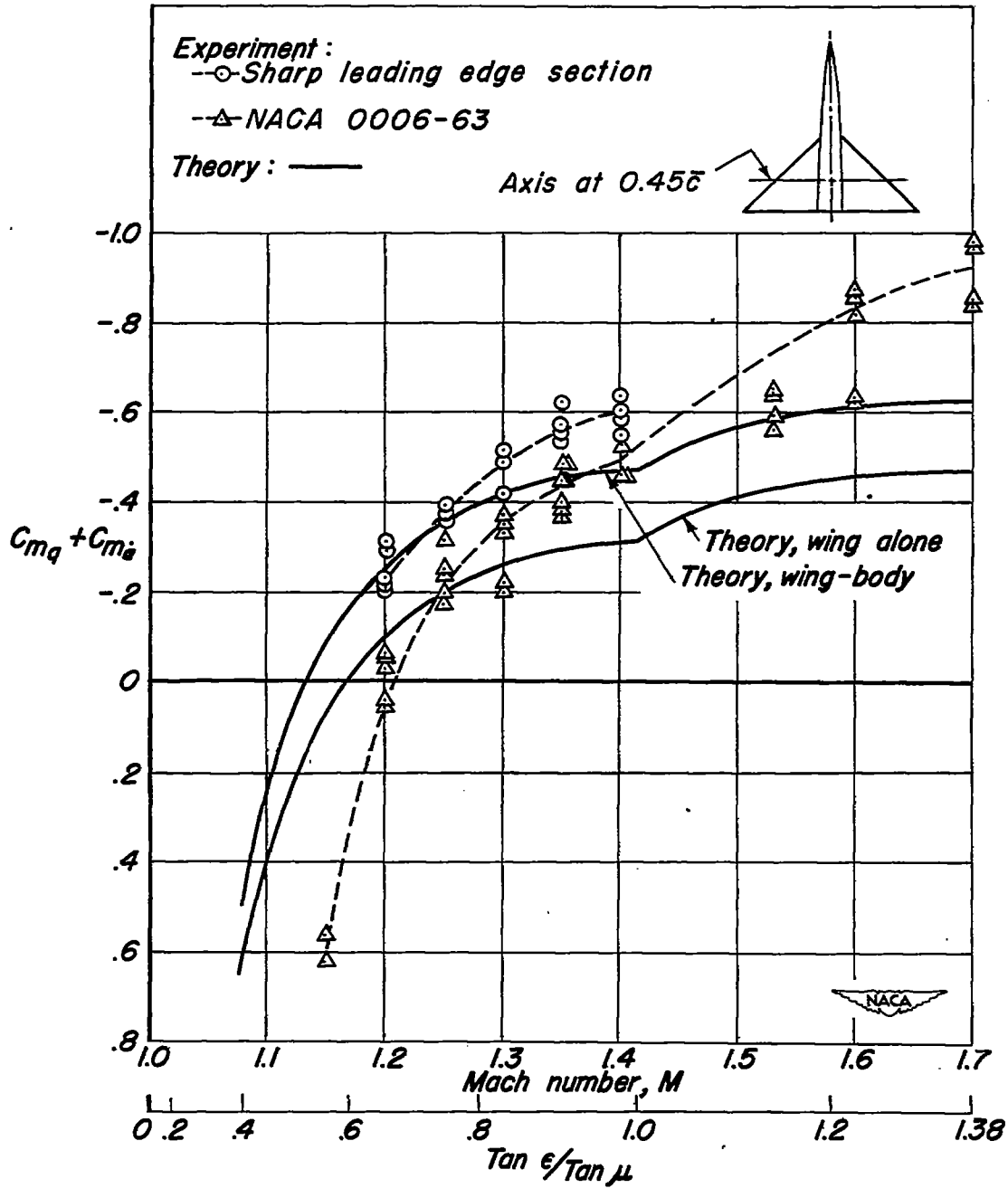

(b) $\alpha = 5°$

Figure 9.- Concluded.

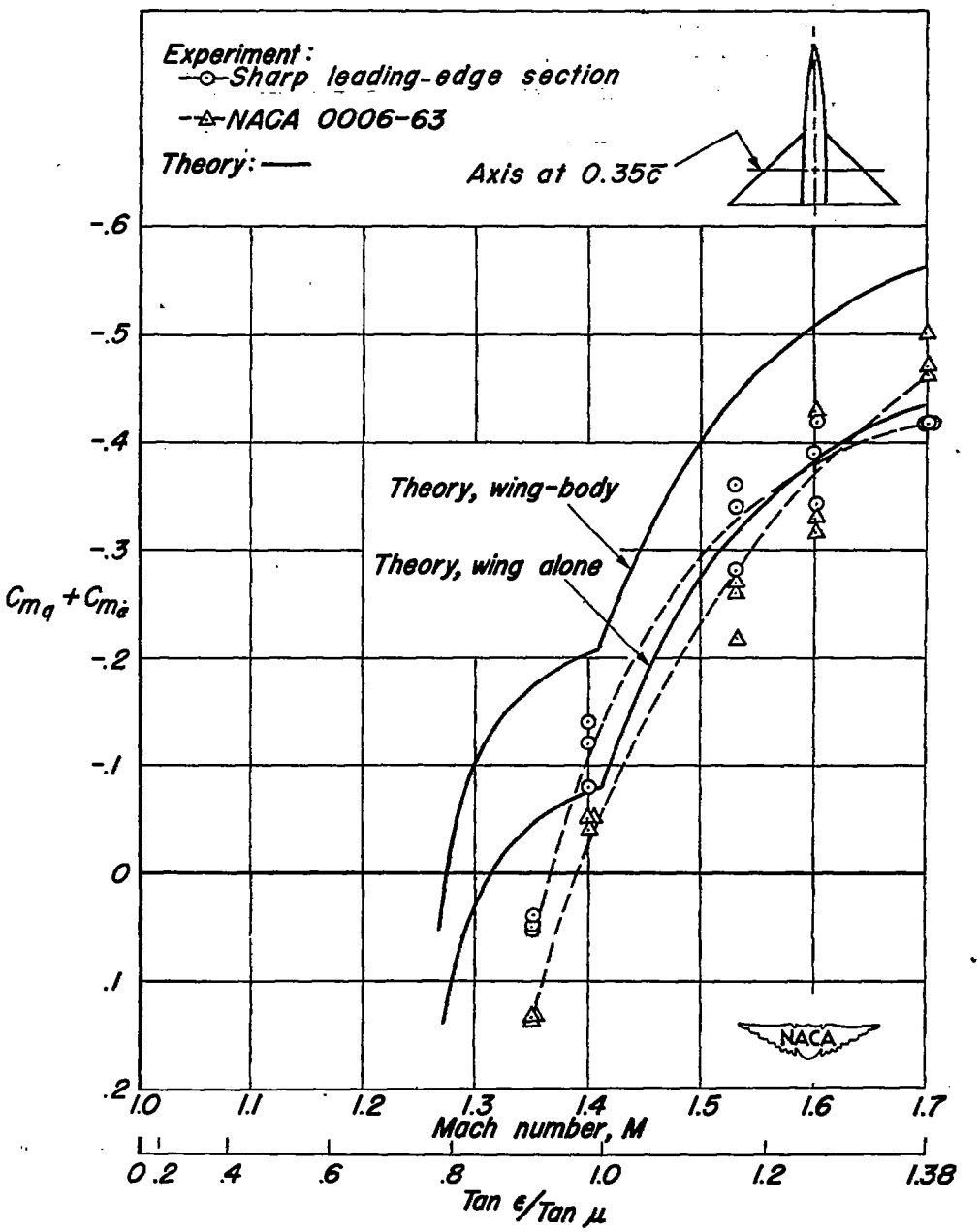

(a) $\alpha = 0°$.

Figure 10.- Experimental damping-in-pitch coefficients for the triangular-wing-body combination at $\alpha = 0°$ and 5° and axis of rotation at 0.35c̄.

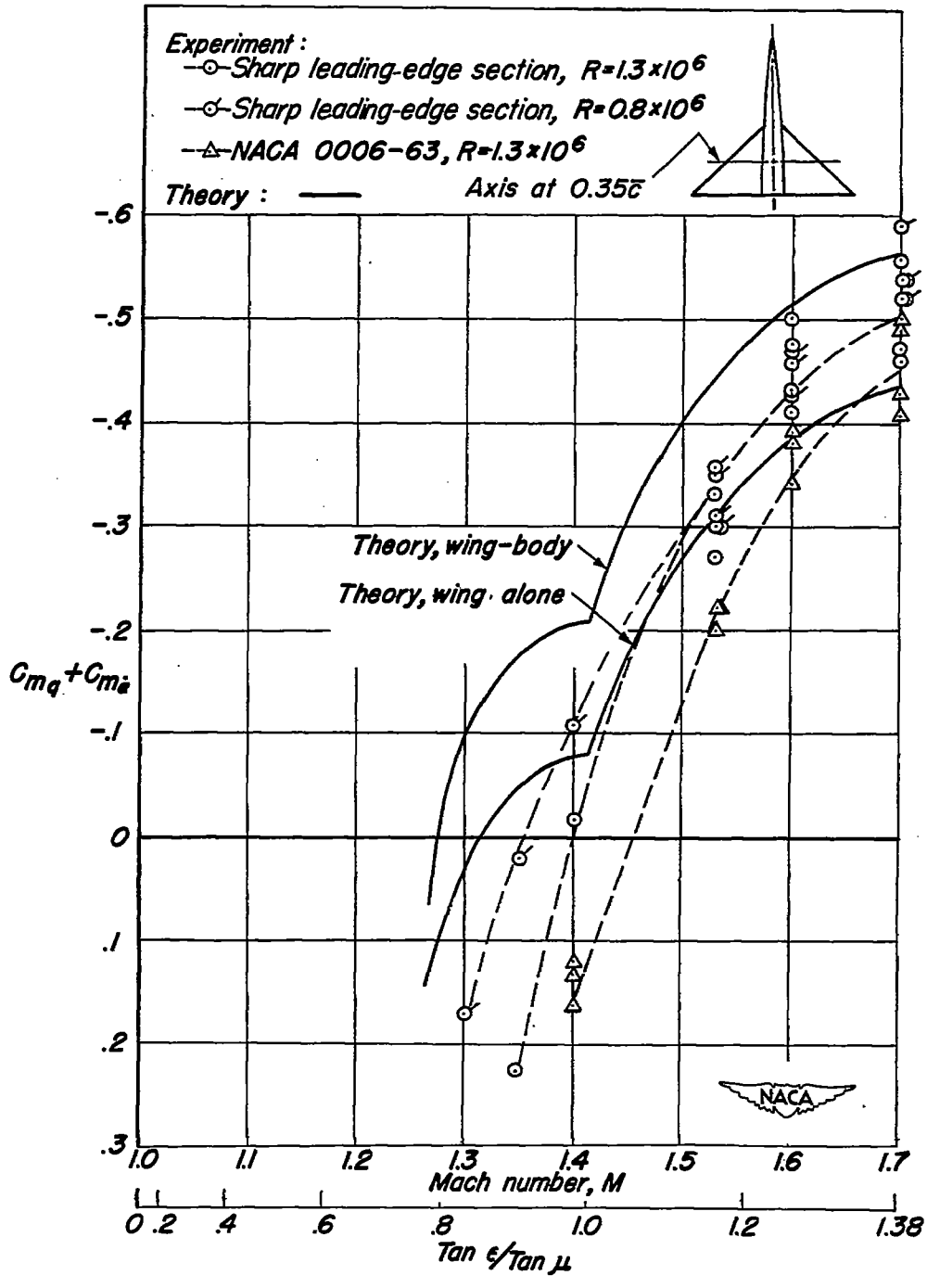

(b) $\alpha = 5°$

Figure 10.- Concluded.

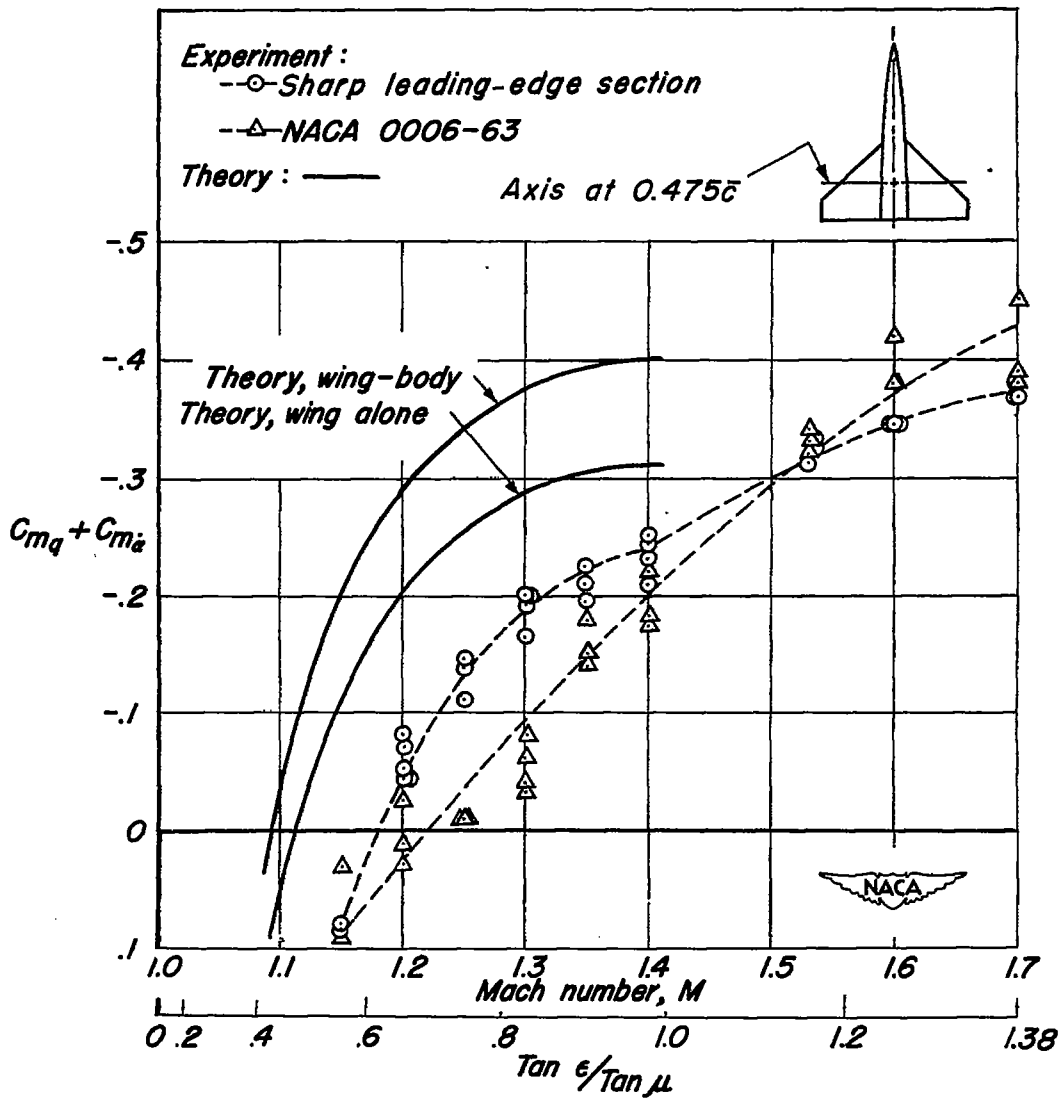

(a) $\alpha = 0°$

Figure 11.- Experimental damping-in-pitch coefficients for the triangular wing with cut-off tips-body combination at $\alpha = 0°$ and 5° and axis of rotation at 0.475$\bar{c}$.

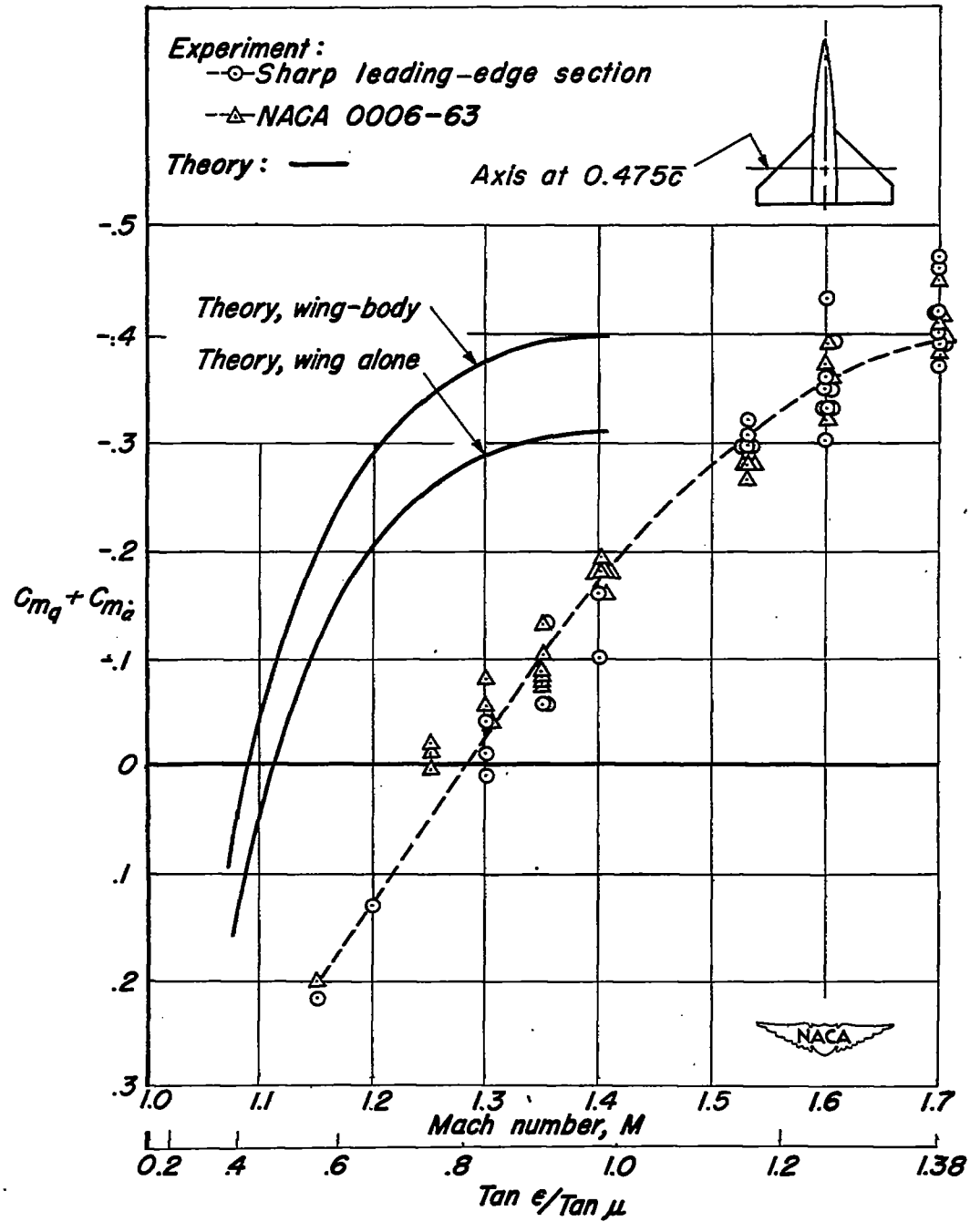

(b) $\alpha = 5°$

Figure 11.- Concluded.

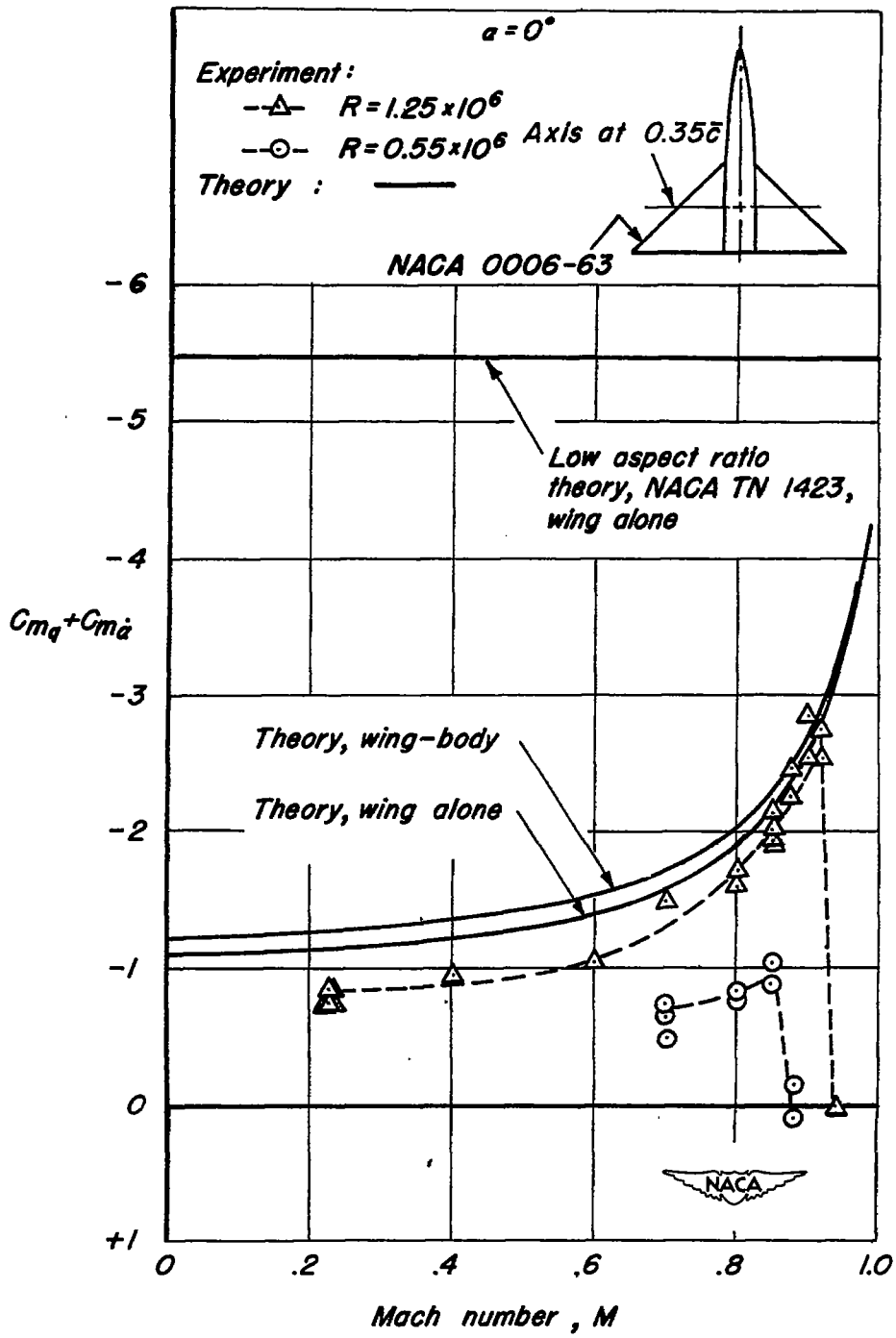

Figure 12.- Experimental damping-in-pitch coefficients at subsonic speeds for the NACA 0006-63 triangular-wing-body combination at $\alpha = 0°$ and axis of rotation at $0.35\bar{c}$.

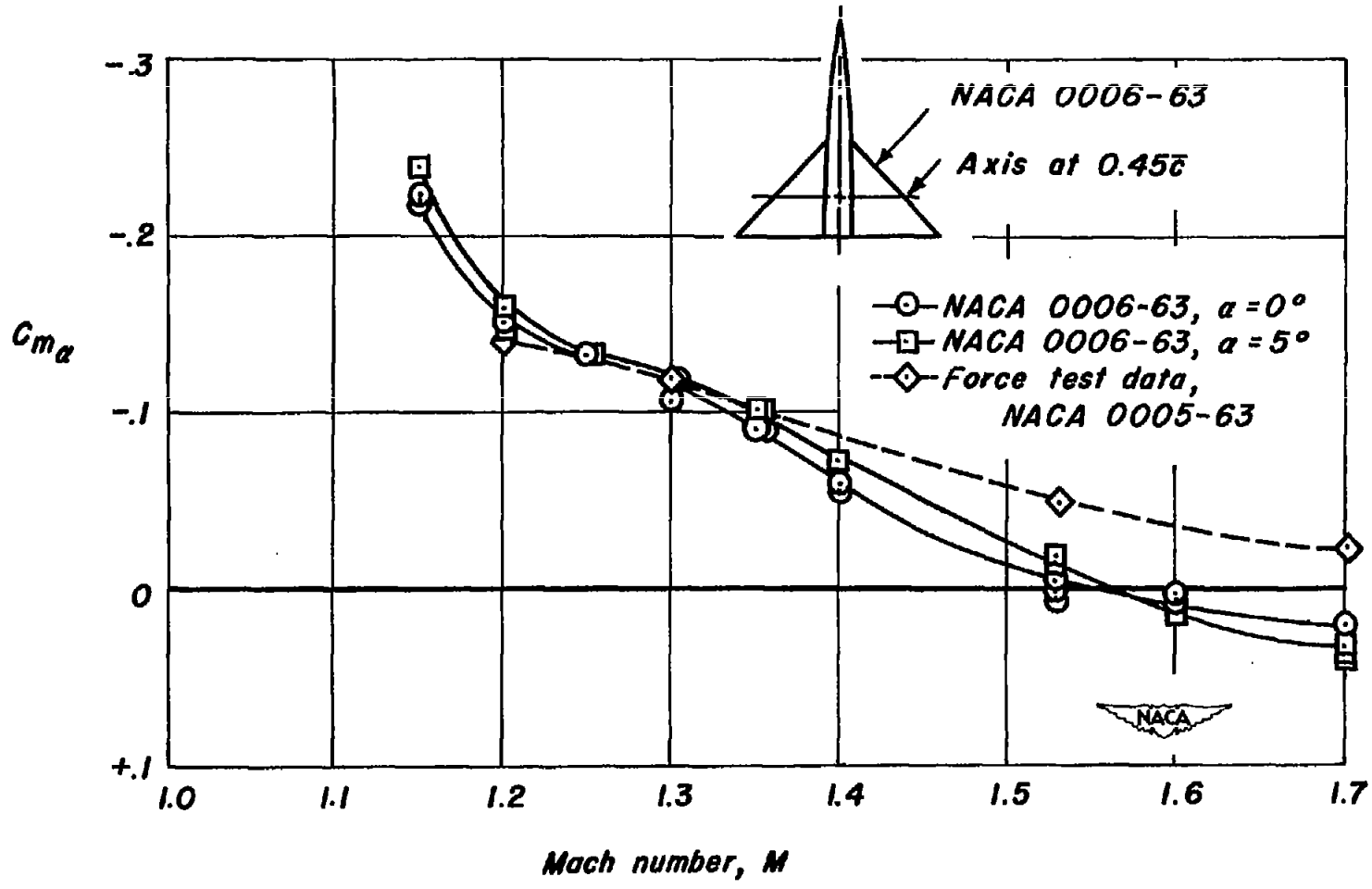

Figure 13.- Experimental pitching-moment coefficients for the round-leading-edge-section triangular-wing-body combination at α = 0° and 5° and axis of rotation at 0.45c̄.

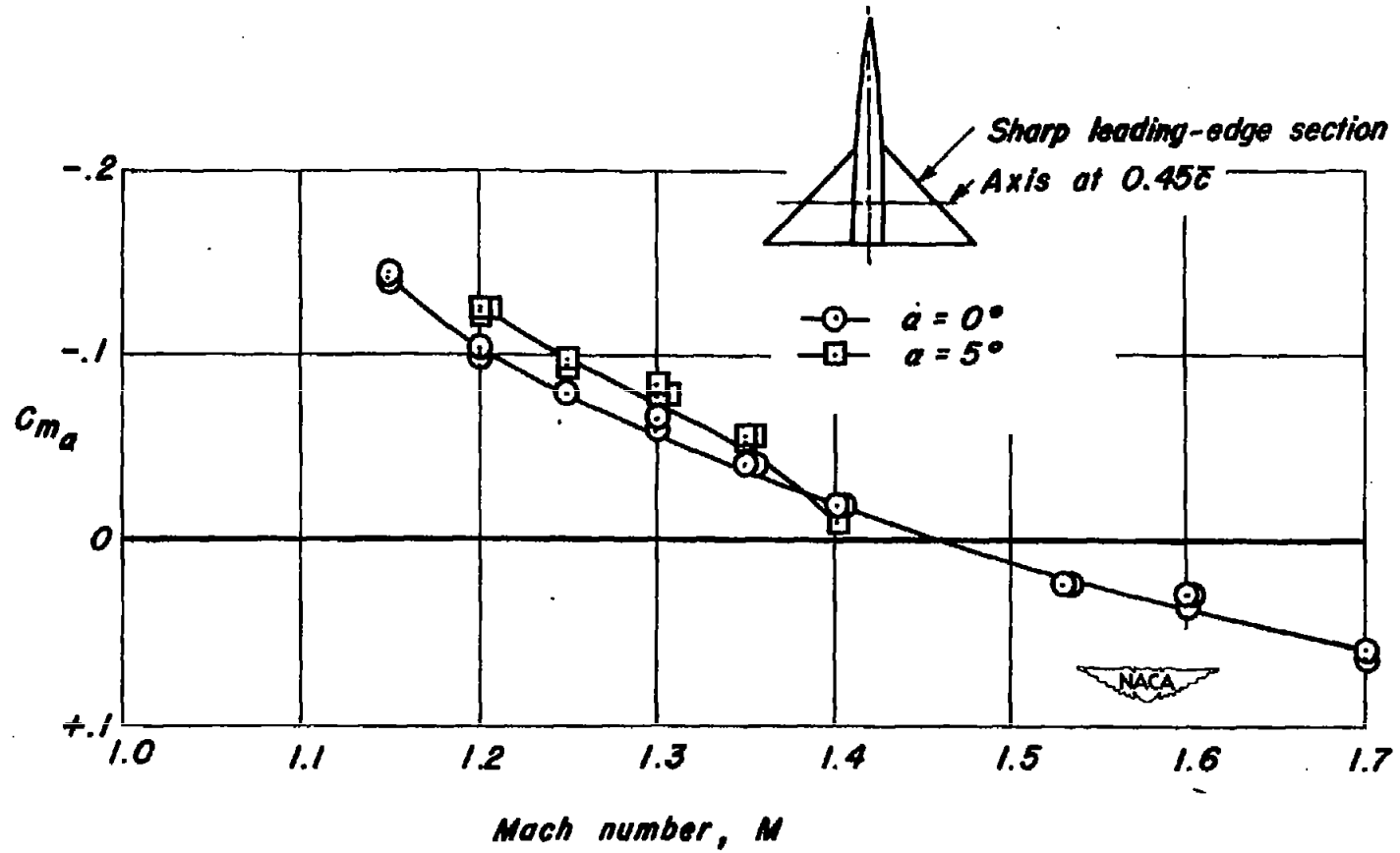

Figure 14.– Experimental pitching-moment coefficients for the sharp leading-edge section triangular-wing–body combination at $\alpha = 0°$ and $5°$ and axis of rotation at $0.45\bar{c}$.

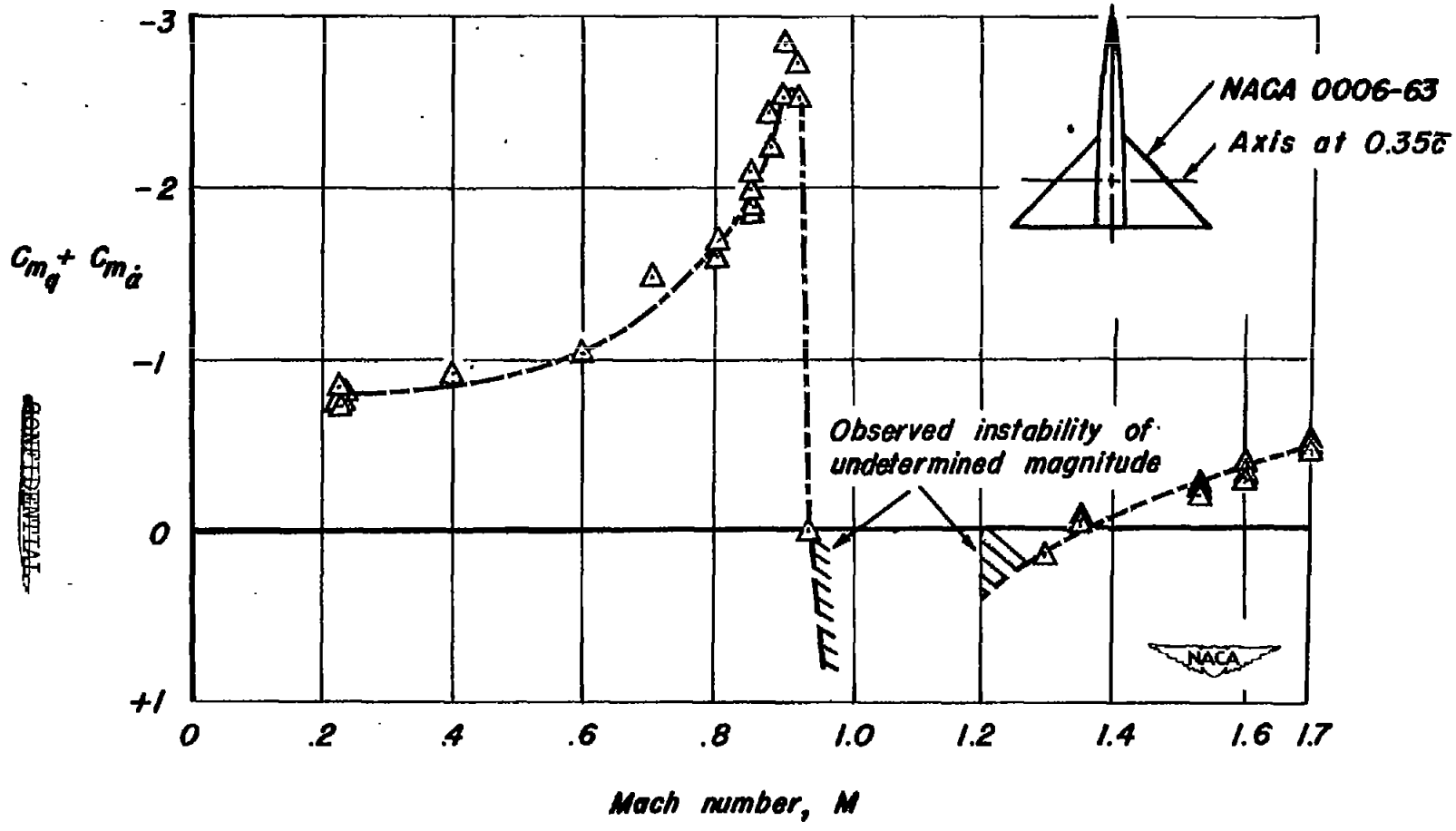

Figure 15.– Experimental damping-in-pitch coefficients at subsonic and supersonic speeds for the NACA 0006-63 section triangular-wing–body combination at $\alpha = 0°$ and axis of rotation at 0.35$\bar{c}$.

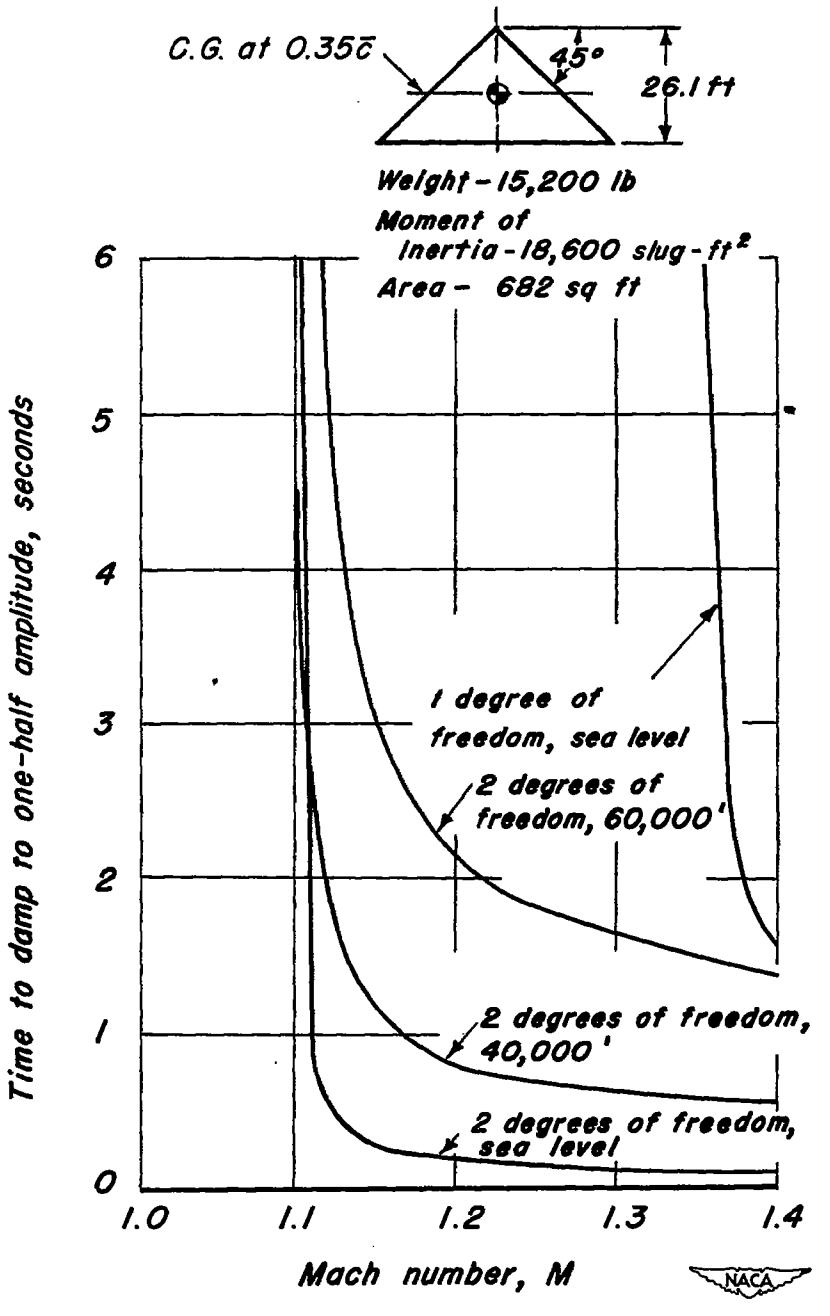

Figure 16.– Comparison of the theoretical time for a short-period pitching oscillation to damp to one-half amplitude at various altitudes for one and two degrees of freedom for a 45° triangular-wing aircraft with center of gravity at 0.35c̄.

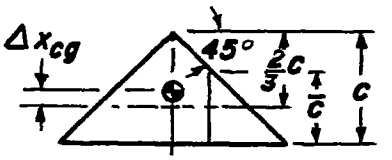

Center of gravity at Δx_{cg}
Weight 15,200 lb
Moment of inertia 18,600 slug-ft^2
Area 682 sq ft

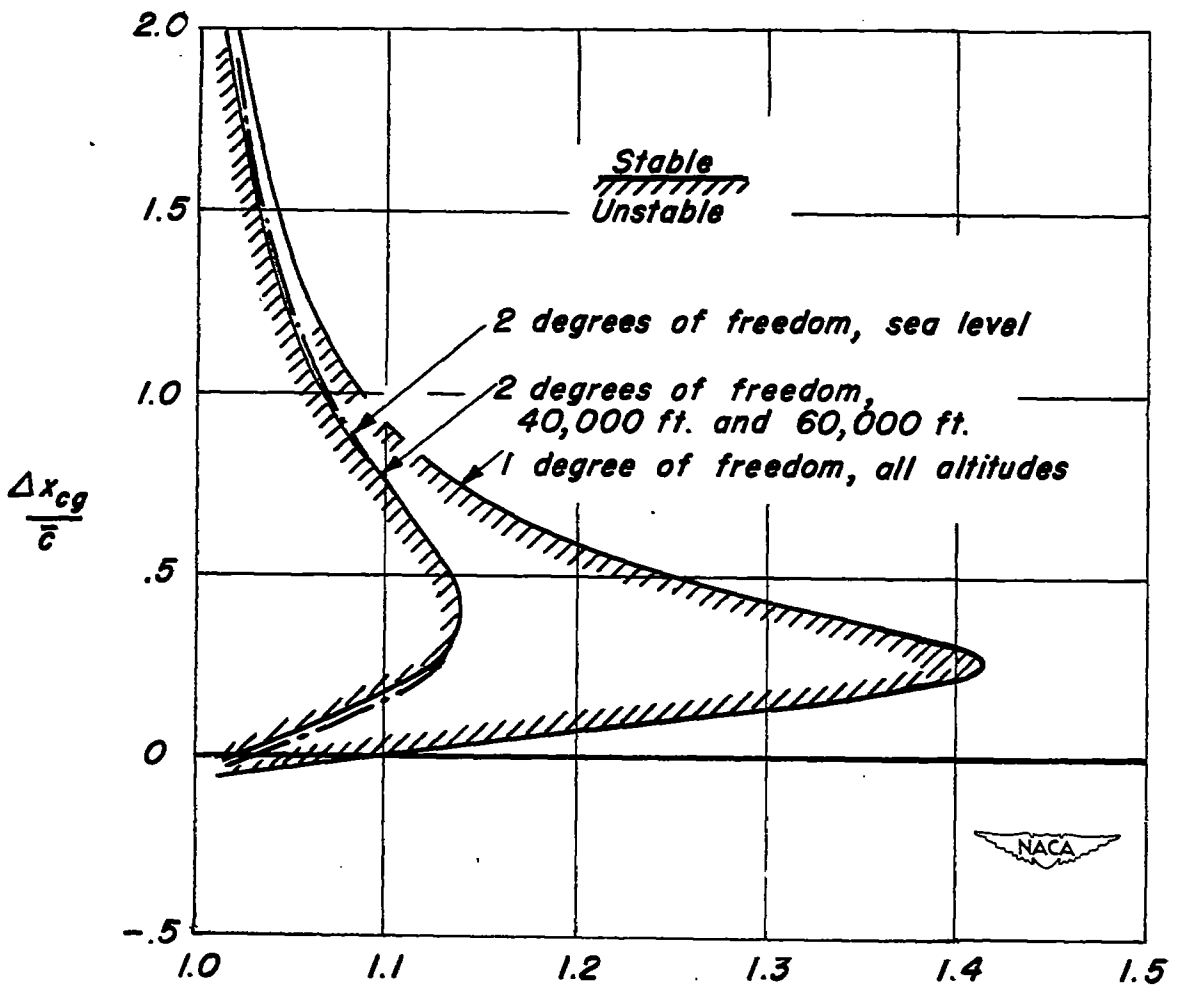

Figure 17.– Comparison of theoretical short-period pitching stability boundaries at various altitudes for one and two degrees of freedom for a 45° triangular-wing aircraft.

CONFIDENTIAL